Cosmological neutrino mass: a frequentist overview in light of DESI

Journal of Cosmology and Astroparticle Physics
An IOP and SISSA journal

Received: *July 30, 2025*
Revised: *October 31, 2025*
Accepted: *November 24, 2025*
Published: *January 22, 2026*

Cosmological neutrino mass: a frequentist overview in light of DESI

D. Chebat et al.
Full author list at the end of the paper

E-mail: domitille.chebat@cea.fr

Abstract: We derive constraints on the neutrino mass using a variety of recent cosmological datasets, including DESI BAO, the full-shape analysis of the DESI matter power spectrum and the one-dimensional power spectrum of the Lyman-α forest (P1D) from eBOSS quasars as well as the cosmic microwave background (CMB). The constraints are obtained in the frequentist formalism by constructing profile likelihoods and applying the Feldman-Cousins prescription to compute confidence intervals. This method avoids potential prior and volume effects that may arise in a comparable Bayesian analysis. Parabolic fits to the profiles allow one to distinguish changes in the upper limits from variations in the constraining power σ of the different data combinations. We find that all profiles in the ΛCDM model are cut off by the $\sum m_\nu \geq 0$ bound, meaning that the corresponding parabolas reach their minimum in the unphysical sector. The most stringent 95% C.L. upper limit is obtained by the combination of DESI DR2 BAO, *Planck* PR4 and CMB lensing at 53 meV, below the minimum of 59 meV set by the normal ordering. The corresponding constraining power σ is 43 meV, which highlights the importance of the cut-off by negative values in the determination of the upper limit. Extending ΛCDM to non-zero curvature and w_0w_aCDM relaxes the constraints past 59 meV again, but only w_0w_aCDM exhibits profiles with a minimum at a positive value. Additionally, we extend the formalism to constrain the lightest neutrino mass. For DESI DR2 BAO, *Planck* PR4 and CMB lensing, we find confidence limits at 20 and 19 meV for normal and inverted ordering, respectively. Using a combination of DESI DR1 full-shape, BBN and eBOSS Lyman-α P1D, we successfully constrain the neutrino mass independently of the CMB. This combination yields $m_\mathrm{l} \leq 97$ and 98 meV in the normal and inverted orderings, and total neutrino mass $\sum m_\nu \leq 285$ meV (95% C.L.). The addition of DESI full-shape or Lyman-α P1D to CMB and DESI BAO results in small but noticeable improvement of the constraining power of the data. Lyman-α free-streaming measurements especially improve the constraint. Since they are based on eBOSS data, this sets a promising precedent for upcoming DESI data.

https://doi.org/10.1088/1475-7516/2026/01/041

JCAP01(2026)041

KEYWORDS: cosmological parameters from LSS, Frequentist statistics, neutrino masses from cosmology

ARXIV EPRINT: 2507.12401

JCAP01(2026)041

Contents

JCAP01(2026)041

1 Introduction

Neutrino oscillations were first observed with solar neutrinos [1–7] and confirmed with atmospheric neutrinos [8–12], accelerators [13–19], and reactor experiments [20–24]. By convention, the neutrino masses are labeled m_1, m_2 and m_3, with $m_1 < m_2$. The collective experimental results (see Particle Data Group [25]) show that at least two of the neutrinos have non-zero masses. The oscillation experiments are sensitive to the difference between squared masses of the neutrinos, $\Delta m^2_{21} \sim 7.5 \times 10^{-5}\,\mathrm{eV}^2$ and $|\Delta m^2_{32}| \sim 2.5 \times 10^{-3}\,\mathrm{eV}^2$. Thus, two of the masses, m_1 and m_2, are close to each other, while m_3 is either larger than m_1 and m_2 ($m_1 < m_2 < m_3$), referred to as normal ordering (NO), or smaller than m_1 and m_2 ($m_3 < m_1 < m_2$), referred to as inverted ordering (IO). By setting the lightest of the three masses to 0, one can determine the smallest possible total mass $\sum m_\nu$ allowed by either ordering,

$$\left(\sum m_\nu\right)^{\mathrm{NO}} > (58.980 \pm 0.304) \times 10^{-3}\,\mathrm{eV}, \quad \left(\sum m_\nu\right)^{\mathrm{IO}} > (99.824 \pm 0.581) \times 10^{-3}\,\mathrm{eV}. \quad (1.1)$$

A cosmic neutrino background with a present-day temperature of 1.9 K and number density 340 cm^{-3} is a central prediction of the standard model of cosmology (ΛCDM), and while not directly observed, is essential in the understanding of Big-Bang Nucleosynthesis (BBN), the cosmic microwave background (CMB) anisotropies, and large scale structure in the Universe (see J. Lesgourgues and L. Verde in section 26 of [25]). Neutrinos uniquely behave as radiation at the time of CMB acoustic oscillations and as dark matter at the time of structure formation. At least two of the three species of cosmic neutrinos are non-relativistic today. Cosmological data are sensitive to neutrino masses through gravitational effects, providing a remarkable connection between particle physics and cosmology.

Cosmology is primarily sensitive to $\sum m_\nu$, and largely insensitive to the individual masses themselves [26–30], providing complementary information to that from neutrino oscillations. In the very early universe, neutrinos have large kinetic energies and are highly relativistic. As time passes, they eventually slow down enough to become non-relativistic, and start contributing to the matter density $\rho_\mathrm{m}(z)$ rather than to the radiation density $\rho_\mathrm{r}(z)$. Neutrinos become non-relativistic when their average momentum approaches their mass. The redshift z_ν at which this transition takes place depends on neutrino masses: a neutrino of mass m_ν transitions at $z_\nu = m_\nu/(53\times10^{-5}\,\mathrm{eV}) - 1$ [25]. For $m_\nu = 50\,\mathrm{meV}$, $z_\nu \sim 100$. The transition from relativistic to non-relativistic neutrinos, thus, happens in the time span between recombination and large-scale structure formation, during the dark matter domination.

A direct consequence of this transition is that, at fixed Ω_m and H_0, the matter density before the transition $\rho_\mathrm{m}(z \gg z_\nu)$ is lower in the case of massive neutrinos than for massless ones. Since the redshift evolution of the expansion parameter $H(z)$ during matter domination is ruled by $\rho_\mathrm{m}(z)$, the value of the neutrino mass affects the angular diameter distance

$$d_\mathrm{A}(z) = \frac{1}{1+z}\int_0^z \mathrm{d}z' \frac{c}{H(z')}. \tag{1.2}$$

This is referred to as the geometrical effect. Baryon acoustic oscillation (BAO) measurements from the Dark Energy Spectroscopic Instrument (DESI) [31–34] probe the angular diameter distance at redshifts $z \ll z_\nu$. Conversely, the determination of the peak scale in CMB surveys such as *Planck* [35–37] or the Atacama Cosmology Telescope (ACT) [38] measures $d_\mathrm{A}(z)$ well before the non-relativistic transition. Individually, neither of these probes are able to constrain the geometrical effect of the neutrino mass. The BAO measurement by DESI only spans redshifts at which the transition has long taken place; as for the CMB, the impact of the neutrino mass is degenerate with the late time expansion history and Ω_m. However, their combination probes $d_\mathrm{A}(z)$ over a range of redshifts that encompasses the non-relativistic transition, and the DESI measurement breaks the degeneracies in the CMB. The combination of BAO and CMB data is thus sensitive to the neutrino mass by means of the geometrical effect.

Another consequence of non-relativistic neutrinos is that they participate in clustering. After the non-relativistic transition, neutrinos behave as hot dark matter. Thus, unlike cold dark matter and baryons, neutrinos have a large enough velocity dispersion that they free-stream at small scales and only engage in clustering at scales above some free-streaming scale λ_fs. This results in a suppression of power in the matter power spectrum at scales below λ_fs, compared to massless neutrinos [39–43]. This effect is commonly referred to as

JCAP01(2026)041

the free-streaming or small-scale suppression effect. In current cosmological datasets, it is measurable in two ways. The reduced clustering weakens the lensing of CMB photons [44], measured by *Planck* and ACT [45–48]. Additionally, improvements in perturbation theory models have allowed exploitation of the full-shape information from large-scale structure (LSS) to constrain the neutrino mass through the measurement of free-streaming [40, 42, 43].

In this work, we perform a frequentist analysis based on profile likelihoods [49] to determine constraints on the neutrino mass from different combinations of cosmological likelihoods. The profile method enables convenient visual comparison between datasets, and provides information on the statistical strength of the data even in situations where the profile is cut off by the physical $\sum m_\nu > 0$ bound. Other works have implemented neutrino mass models that can be effectively extended to negative masses [50–53] to deal with this limitation. In our case, although the profiles are graphically extrapolated into the negative sector for ease of visual comparison, computations are strictly kept to $\sum m_\nu > 0$, and the upper limit computations take this lower bound into account. We also derive upper limits constrained by 0.059 eV and 0.100 eV lower bounds, according to the minima imposed by normal and inverted orderings presented in eq. (1.1).

The rest of our work is organized as follows: in section 2, we describe the frequentist framework used to build and analyze the profile likelihoods and derive the corresponding confidence limits. Section 3 lists the various datasets and codes used for the analysis. In section 4, we report results based on datasets combinations that strongly rely on geometrical information and where small-scale suppression measurement stems from CMB lensing measurements. Section 5 focuses on exploiting free-streaming information from full-shape measurements of the matter power spectrum. Finally, in section 6, we consider individual neutrino masses instead of $\sum m_\nu$. We investigate the impact of the mass splitting modeling in the Boltzmann solver when computing profile likelihoods, and consider the impact of shifting minimal $\sum m_\nu$ to that allowed by normal or inverted ordering. We summarize our findings and conclude in section 7.

2 Inference methodology

2.1 Profile likelihoods

We use a frequentist approach to report constraints on the sum of neutrino masses $\sum m_\nu$. Specifically, we construct profile likelihoods by performing likelihood maximization over a span of $\sum m_\nu$ values. Let $\mathscr{L}\left(\sum m_\nu, \mathscr{C}, \mathscr{N}\right)$ be the likelihood of interest where $\mathscr{C}$ is our cosmological basis, excluding $\sum m_\nu$, and $\mathscr{N}$ are the possible nuisance parameters associated with the likelihood. The profile likelihood is defined as a function of $\sum m_\nu$: for a fixed neutrino mass, it is the result of the maximization of the likelihood over all other parameters — cosmological or nuisance. It is generally considered in log-space, so for a Gaussian likelihood, this corresponds exactly to a χ^2 function, and we refer to the profile likelihoods as $\chi^2(\sum m_\nu)$. Since we have a one-dimensional problem, the profiles are simple parabolas. In the rest of this work, we perform minimization of $-2\log\mathscr{L}$ for several fixed values of $\sum m_\nu$ and fit the resulting points to a parabola.

The next step is to build a likelihood ratio for the best $\sum m_\nu$, the neutrino mass that minimizes the profile. Normally, this amounts to reporting $\Delta\chi^2$ by subtracting the parabola

JCAP01(2026)041

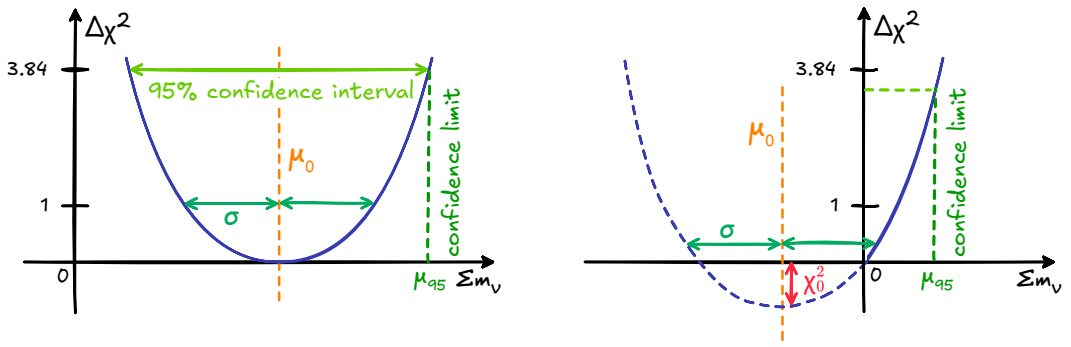

Figure 1. Profile likelihoods in the regular and interrupted case, with parabolic fit parameters.

minimum (see figure 1). In the case of the neutrino mass, however, there is a natural lower bound at $\sum m_\nu = 0$ beyond which we cannot proceed. Furthermore, considering the results of oscillation experiments, one can even argue for a lower bound at 59 or 100 meV for the normal and inverted orderings, respectively. Since cosmological constraints tend to favor very low neutrino masses, most of the profiles we present in sections 4 and 5 are actually cut off by the $\sum m_\nu = 0$ bound before the minimum of the parabola. This has been observed in previous works on neutrino mass profile likelihoods [54, 55], and is analogous to the Bayesian posteriors [34, 53, 56] that do not peak at positive values. Since the minimum of the parabola is in a forbidden region, we instead report $\Delta\chi^2$ as the difference between χ^2 and the minimal computed χ^2. In the most frequent case where we can only probe a branch of the parabola, this reduces to

$$\Delta\chi^2\left(\sum m_\nu\right) = \chi^2\left(\sum m_\nu\right) - \chi^2\left(\sum m_\nu = 0.005\,\text{eV}\right), \tag{2.1}$$

where the last term has been set to an arbitrary lower mass bound near zero of 0.005 eV. We fit $\Delta\chi^2$ to a parabola of the form $x \mapsto (x-\mu_0)^2/\sigma^2 - \chi_0^2$, and report μ_0 and σ. The latter can directly be interpreted as the constraining power of the data. In the case where the parabola is cut off, the offset χ_0^2 corresponds to the tension between $\sum m_\nu = 0$ and the parabola's minimum. Graphically, we extend the profile into the $\sum m_\nu \leq 0$ sector, which allows for easy visual comparison of different profiles. A simplified example is shown in figure 1.

For a standard, uninterrupted profile, 95% C.L. limits can be reported by finding the mass such that $\Delta\chi^2 = 3.84$. In the case of cut-off profiles, the overlap between the parabola and negative values make this reasoning invalid. Instead, we report 95% C.L. limits following the Feldman-Cousins prescription [57] as described in section 2.2. Nevertheless, unless μ_0 is negative and several σ away from zero, $\Delta\chi^2 = 3.84$ is a reasonable proxy for the 95% C.L. limit. We thus display the $\Delta\chi^2 = 3.84$ line on plots to aid with visual comparison.

2.2 Confidence limits

In the case of the neutrino mass, there exists a physical limit $\sum m_\nu > 0$. Because current constraints are very close to this boundary, the classical confidence interval often overlaps with negative values, and is thus rendered incorrect. In [57], the authors describe the construction of a corrected confidence interval for a Gaussian likelihood whose mean should be positive,

JCAP01(2026)041

often called the Feldman-Cousins prescription after the authors. The prescription can be directly followed to build upper limits for the neutrino mass which take into account that $\sum m_\nu$ must be positive.

Current neutrino mass constraints also overlap with oscillation-based lower limits. It is thus desirable to build modified upper limits with physical boundaries $\sum m_\nu \geq 59\,\text{meV}$ (NO) and $\sum m_\nu \geq 100\,\text{meV}$ (IO), which we do by adapting the Feldman-Cousins prescription as described below.

Following the convention used in [57], let μ be the neutrino mass, whose true value is unknown, and x the corresponding observable such that the likelihood $\mathscr{P}(x|\mu)$ (i.e., the probability of measuring x given some conditioning μ) is a Gaussian with mean μ and scale 1. We add the constraint that μ must be greater than some boundary μ_inf (in practice 0, 59 or 100 meV), while x may take values below μ_inf.[1]

We define μ_best as the physically allowed $\mu \geq \mu_\text{inf}$ that maximizes the likelihood of a given observed x. This amounts to $\mu_\text{best} = \max(x, \mu_\text{inf})$. We then consider the ratio $R(x,\mu)$ of the likelihood $\mathscr{P}(x|\mu)$ to its maximum $\mathscr{P}(x|\mu_\text{best})$ as an ordering principle to construct acceptance intervals:[2]

$$R(x,\mu) = \frac{\mathscr{P}(x|\mu)}{\mathscr{P}(x|\mu_\text{best})} = \begin{cases} \mathrm{e}^{-\frac{1}{2}(x-\mu)^2} & \text{if } x \geq \mu_\text{inf} \\ \mathrm{e}^{-\frac{1}{2}(x-\mu)^2} / \mathrm{e}^{-\frac{1}{2}(\mu_\text{inf}-\mu)^2} & \text{if } x < \mu_\text{inf} \end{cases} \tag{2.2}$$

For a coverage probability α and a given μ, the acceptance interval is $[x_1, x_2]$ such that $R(x_1,\mu) = R(x_2,\mu)$ and $\int_{x_1}^{x_2} R(x,\mu)\,\mathrm{d}x = \alpha$. Using these acceptance intervals, one can then determine confidence intervals $[\mu_1, \mu_2]$ for a measured x_0. This confidence interval is the set of all μ such that x_0 belongs to the corresponding acceptance interval.

The reasoning can be applied to any Gaussian likelihood of scale $\sigma \neq 1$ by normalizing it and scaling the resulting confidence interval again. In the following, we will use this construction at $\alpha = 0.95$ with $\mu_\text{inf} = 0$, 59 and 100 meV to report 95% confidence intervals named μ_{95}, $\mu_{95}^{(\text{NO})}$ and $\mu_{95}^{(\text{IO})}$ respectively.

Applied to the profile likelihoods computed in this work, the procedure is the following: instead of an observed x_0, we consider the parabolic fit parameter μ_0. For our choice of μ_inf, we compute the confidence interval that corresponds to the minimum of the parabola μ_0, accounting for $\sigma \neq 1$. In all cases in this work, μ_0 is small enough that the confidence interval takes the form $[\mu_\text{inf}, \mu_{95}]$, so that only the value of the upper limit is of interest. Figure 2 exhibits how this upper limit varies as a function of the minimum location μ_0, for a fixed constraining power σ and different boundaries μ_inf. It showcases that for current measurements of the neutrino mass, for which μ_0 can be lower than μ_{inf} by a few σ, the upper limit derived from the Feldman-Cousins prescription is a non-negligible correction to the standard Gaussian one.

[1] A simple context in which this may arise is an experiment measuring some amplitude A, with known background B. If the measured data just stochastically happen to average below the background value B, one would measure negative amplitude ($x = A^{(\text{measured})} < 0 = \mu_\text{inf}$), even though its true value should theoretically be positive ($\mu = A^{(\text{theory})} > 0 = \mu_\text{inf}$).

[2] In the standard case with no physical boundary, $\mu_\text{best} = x$ and $R(x,\mu) \propto \mathscr{P}(x|\mu)$. The acceptance interval is symmetric and centered in $x = \mu$.

JCAP01(2026)041

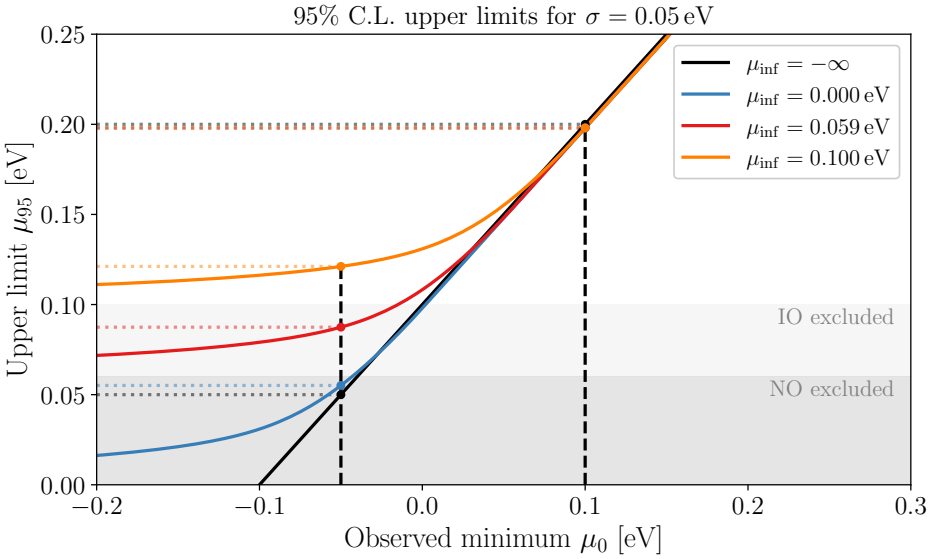

Figure 2. 95% C.L. upper limit of a profile with constraining power $\sigma = 0.05\,\mathrm{eV}$, as a function of the profile's minimum position μ_0. The different colors correspond to different values of the physical boundary μ_{inf}, and black corresponds to the standard, boundary-less case. The dashed lines represent two hypothetical example measurements μ_0. When the measurement is well below the boundary (e.g., the dashed line at $\mu_0 = -0.05\,\mathrm{eV}$), the upper limit is strongly increased compared to the boundary-less case, and confined at values above the boundary $\mu_{95} > \mu_{\mathrm{inf}}$. However, for a measurement above μ_{inf} (e.g., the dashed line at $\mu_0 = 0.10\,\mathrm{eV}$), the upper limits almost coincide with the boundary-less case.

3 Data and software

Cosmological inference is performed in a 7-parameter ΛCDM+$\sum m_\nu$ model, comprised of Ω_{m}, H_0, $\ln(10^{10}A_{\mathrm{s}})$, n_{s}, $\Omega_{\mathrm{b}}h^2$, τ and $\sum m_\nu$, which refer to the matter energy density fraction, the Hubble parameter, the logarithm of the amplitude of primordial density fluctuations, the spectral index, the baryon energy density fraction times h^2, where $h = H_0/100\,\mathrm{km\,s^{-1}\,Mpc^{-1}}$, the reionization optical depth, and the summed neutrino masses, respectively. In the following, we detail data, data products and codes used in our analysis as well as the corresponding nomenclature for the article.

3.1 Cosmological likelihoods

Cosmic Microwave Background. We make use of cosmic microwave background (CMB) measurements by *Planck* [35] and ACT [38]. We combine *Planck* low-ℓ EE and TT likelihoods with high-ℓ TT, TE, and EE. The low-ℓ data products are the `Commander` and `SimAll` likelihoods from the 2018 *Planck* data release [35]. For high-ℓ information, we use both 2018 (PR3) and 2020 (PR4) TTTEEE likelihoods. In the following, *Planck* PR3 refers to the official `plik` likelihood from the 2018 data release [35], while *Planck* PR4 corresponds to the `CamSpec` likelihood based on the *Planck* 2020 analysis [58].

We also use a compressed, foreground-marginalized likelihood for the ACT DR6 high-ℓ TTTEEE data [38] referred to as `ACT-lite`.[3] We follow the ACT collaboration and

[3] https://github.com/ACTCollaboration/DR6-ACT-lite.

JCAP01(2026)041

combine this likelihood with the low-ℓ `Srol12` *Planck* EE likelihood[4] described in [59]. This combination is referred to as `ACT-lite` in the following.

Some profiles include isolated *Planck* 2018 information on n_s, $\ln(10^{10}A_\mathrm{s})$, or both. This corresponds to the ΛCDM constraints reported on these parameters in [35], implemented as Gaussian likelihoods.

- $n_{\mathrm{s},\ 1\sigma}$ corresponds to the *Planck* constraint.
- $n_{\mathrm{s},\ 10\sigma}$ is a relaxed version of the former, with a standard deviation ten times greater.
- $n_{\mathrm{s},\ 1\sigma}\ +\ A_s$ implements 1-σ constraints for both n_s and $\ln(10^{10}A_\mathrm{s})$ as well as the corresponding covariance.

CMB lensing. In addition to TT, TE, EE information on the CMB, we include CMB lensing information both from *Planck* PR4 and ACT DR6 [45, 46] combined in one likelihood[5] as described in [48]. CMB lensing is included by default in the profiles labeled *Planck* PR3, *Planck* PR4, and ACT-lite.

Galaxy clustering. We use galaxy clustering measurements by DESI to constrain the neutrino mass. DESI is a spectroscopic instrument that uses 5000 robotic fiber positioners to capture target spectra over 7 deg^2 field of view [32, 60–63]. Targets are selected from the public Legacy Surveys [64, 65] and their spectra are classified and processed into a redshift catalog [66–68]. After the first round of survey validation for each category of target [69–76], cosmological analysis has been performed based on the contents of the first two data releases, the first of which is now publicly available [77].

Measurements of BAO help constrain the neutrino mass through geometrical information. We employ such measurements from the first two DESI data releases, DR1 [33, 78, 79] and DR2 [34, 80], and will refer to them as DR1 BAO and DR2 BAO. Additionally, we make use of the full-shape likelihood of DESI DR1 [42, 81], which is sensitive to neutrino free-streaming, in combination to the associated BAO measurement. We refer to this combination as DESI FS.

Big Bang nucleosynthesis. Baryon abundance in the universe can be determined from BBN. In the following, we use the constraint $\Omega_\mathrm{b}h^2 = 0.02218 \pm 0.00055$ in ΛCDM from a recent analysis [82], and refer to it as BBN.

Supernovae. We use distance measurements from the sample of type Ia supernovae (SN) published by the *Dark Energy Survey* in their Year 5 data release [83], under the form of the corresponding `Cobaya` likelihood. When included, this likelihood is referred to as DES-Y5. Detailed comparison of the Pantheon+ and Union3 SN data sets has been reported in [53] and they are not used in this work.

[4] Available at https://sroll20.ias.u-psud.fr/ and https://web.fe.infn.it/~pagano/low_ell_datasets/sroll2/.

[5] Specifically, we use the `actplanck_baseline` variant in version `1.2`, available at https://github.com/ACTCollaboration/act_dr6_lenslike.

JCAP01(2026)041

Lyman-α forest. The one-dimensional power spectrum of the Lyman-α forest (P1D) allows probing small-scale suppression of the matter power spectrum. Although DESI has measured the Lyman-α forest P1D [84, 85], the interpretation relies on the emulation of sets of high precision hydrodynamical simulations and is still a work in progress.

In the following, we use the results from two sets of such simulations on the parameters $n_{\rm Lya}$, $A_{\rm Lya}$ of the P1D. Both works use the quasars from Data Release 14 of the *Sloan Digital Sky Survey*, SDSS DR14 [86]. The first is described in [87] and referred to as Taylor, while the second results from the work in [88] and is referred to as Lyssa. Both likelihoods are implemented as compressed information using the chains from [88]; for Lyssa, we use the chain that includes a mean transmission prior. The results of the minimizations that involve either likelihood lie within the cosmological parameter space covered by the respective simulation grids [88–90].

3.2 Inference framework

All likelihoods are implemented in `Cobaya` [91, 92], using the `CAMB` Boltzmann solver [93, 94]. In order to perform the minimization, likelihoods are interfaced with the `Minuit2` [95] minimizer through its Python frontend `iminuit` [96]. The baseline cosmological model is flat ΛCDM in which neutrinos are modeled as three species of degenerate mass. The effect of this assumption of degenerate neutrino masses is explored in section 6.

The minimization is run in a parameter space consisting of the cosmological basis ($\Omega_{\rm m}$, H_0, $\ln(10^{10}A_{\rm s})$, $n_{\rm s}$, $\Omega_{\rm b}h^2$, τ, $\sum m_\nu$) as well as any nuisance parameters required by the likelihoods involved. In section 4.2, we consider extensions to the base ΛCDM+$\sum m_\nu$ model:

- The Chevallier-Polarski-Linder ($w_0w_{\rm a}$CDM) dynamical dark energy [97, 98], in which the equation of state of dark energy is parametrized as $w(z) = w_0 + (z/(1+z))\, w_{\rm a}$.
- A universe with non-zero curvature, where $\Omega_{\rm K}$ is free.

In those cases, we extend the basis to include w_0 and $w_{\rm a}$ or $\Omega_{\rm K}$. Depending on the choice of likelihoods, the dimension of the parameter space for the minimization may range from 8 to more than 40. The cosmological basis has been chosen for easy compatibility with the likelihoods used in this work. It should however be noted that unlike Bayesian inference techniques, such as Markov chain Monte Carlo, minimization — and, thus, profile likelihoods — are invariant under a reparametrization of the parameter basis.

It can happen that the whole cosmological basis is not needed. For instance, in the data combinations of section 5, the function to minimize is completely independent of τ. In such situations, we freeze the parameter in question. The CMB and DESI full-shape likelihoods introduce numerous nuisance parameters. For these, we implement penalties and limits on the explored parameter space as prescribed in their original frameworks. The cosmological parameters are allowed to vary within the domain described in table 1. The nominal observed values of the parameters are summarized by O. Lahav and A. R. Liddle in section 25 of [25].

JCAP01(2026)041

	Ω_m	H_0	$\log A$	n_s	$\Omega_b h^2$	τ	w_0	w_a	Ω_K
Minimum	0.2	60	2.8	0.92	0.015	0.02	-3.0	-3.0	-0.3
Maximum	0.4	90	3.9	1.02	0.03	0.1	0.0	2.0	0.3

Table 1. Minimization domain for each cosmological parameter.

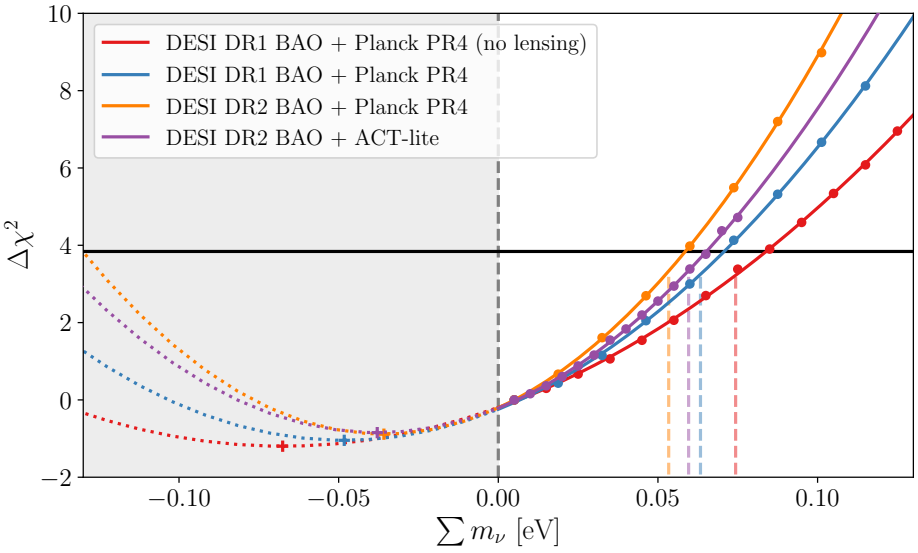

Figure 3. Profile likelihoods for different combinations of BAO with CMB data from *Planck* and ACT. Including lensing information and switching from DESI DR1 BAO to DESI DR2 BAO improves the constraining power of the data, and shifts the minima toward the positive values. Combined, these effects lead to a lower upper limit. Replacing CMB data from *Planck* with that from ACT-lite slightly relaxes the constraint from DESI DR2 BAO + *Planck* PR4 without shifting the parabola.

4 Geometry and small-scale suppression with the CMB

In this section, we present profiles in the ΛCDM and w_0w_aCDM frameworks using combinations of BAO and CMB data. The constraints derive from the geometrical effect as well as measurement of small-scale suppression from the CMB.

4.1 Flat ΛCDM

4.1.1 CMB and DESI BAO

As explained in section 1, combining BAO and CMB data breaks parameter degeneracies specific to each dataset and allows one to constrain the neutrino mass through the geometrical effect. Including CMB lensing information adds sensitivity to the neutrino mass through a different effect, the suppression of small scales in the matter power spectrum. Recent BAO data are available from DR1 and DR2 of DESI, and CMB data from *Planck* and ACT. In figure 3, we compare various combinations of these datasets. Several conclusions can be drawn from one-on-one comparisons of the profiles.

First, in the most constraining combination (DESI DR2 BAO + *Planck* PR4), replacing *Planck* PR4 with ACT-lite yields little difference. The upper limit is slightly increased, which

JCAP01(2026)041

is consistent with results reported by Bayesian analyses [99, 100]. The increase is only due to a slight relaxation of the parabola, whose position does not change. Since a significant part of the ACT likelihood is shared with Planck, including CMB lensing, this is not unexpected.[6]

On the contrary, the switch from DR1 to DR2 BAO and the addition of CMB lensing each cause the parabola minimum to shift, toward the positive. At constant σ, this should cause the upper limit to increase. However, the gain in constraining power offered by these changes is large enough that the upper limit actually decreases in each case. The addition of CMB lensing allows sensitivity to the free-streaming effect, bringing σ down by 13 meV. The upgrade from DR1 to DR2 for the BAO measurement tightens the constraint on $\Omega_{\rm m}$, leading to an 11 meV decrease of σ. In both cases, the improvement in constraining power is higher than the change in upper limit could have suggested.

In the end, the most constraining combination (DESI DR2 BAO + *Planck* PR4) yields $\sigma = 43$ meV and a 95% C.L. limit at $\sum m_\nu < 53$ meV. To put things in perspective, the final design report of DESI originally forecast DESI Y5 to achieve $\sigma \sim 20$ to 30 meV [101]. The tension with regard to positive values, indicated by the vertical offset of the parabola χ^2_0, remains below 1 in all cases and tends to decrease with the inclusion of new data.

In addition to the BAO measurement, we can also use the full-shape information from the DESI data. Like CMB lensing, the full-shape measurement of the power spectrum should contribute to the constraint through the free-streaming effect. We follow the Bayesian analysis in the original DESI publication [42] and consider the combination of DESI full-shape and BAO from DR1 with *Planck* PR3 `plik`. The corresponding profiles are plotted in figure 4. We first note that the change from *Planck* PR3 `plik` to *Planck* PR4 `CamSpec` has very little impact on the profile, save for a slight decrease of the upper limit, also observed in the corresponding Bayesian analyses with DESI DR2 [53].

The addition of full-shape information causes the profile to shift toward the negative by 17 meV, while the constraining power barely improves by 2 meV. As a consequence, the upper limit is pulled down from 68 to 53 meV, just like the DESI DR2 BAO + *Planck* PR4 combination. However, unlike DESI DR2 BAO, the gain from DESI DR1 BAO to full-shape is predominantly driven by the shift of the parabola. At $\sigma = 53$ meV, the data is about as constraining with full-shape as it is without. This indicates that small-scale suppression measurements from DESI full-shape are not competitive with CMB lensing yet. Lastly, in the case of the DESI full-shape profile, there is more significant tension between the parabola's minimum and positive values.

4.1.2 CMB and Lyman-α

Profiles for the combination of CMB, BAO, and Lyman-α P1D are shown in figure 5. The addition of either Lyssa or Taylor information to CMB alone results in a decreased upper limit and a smaller σ. Although the combination with Taylor results in a higher limit (160 meV) than Lyssa (143 meV), it actually carries the tightest constraining power, standing at $\sigma = 102$ meV compared to the 115 meV of Lyssa. This stems from the different directions of the shift of the minima compared to the CMB alone: positive for Taylor and negative for

[6] CMB lensing is a combination of *Planck* and ACT data, see section 3. The lower-ℓ part of the high-ℓ ACT likelihood is taken from *Planck* PR3 [38].

JCAP01(2026)041

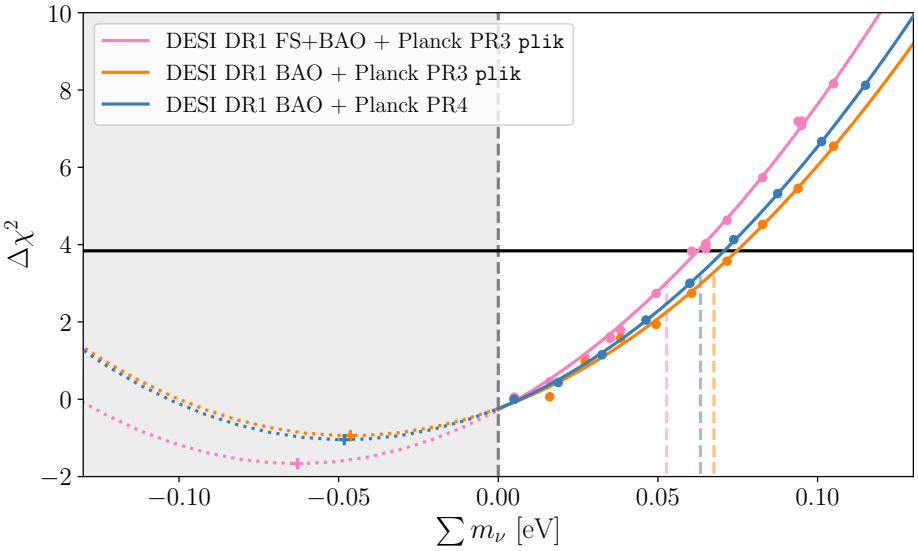

Figure 4. Profile likelihoods for different combinations of DESI BAO and full-shape with CMB data from Planck. The change in *Planck* likelihood, from PR3 `plik` to PR4 `CamSpec`, produces extremely similar results. Adding full-shape information to DR1 BAO shifts the parabola slightly to the negative, with some improvement to the constraining power.

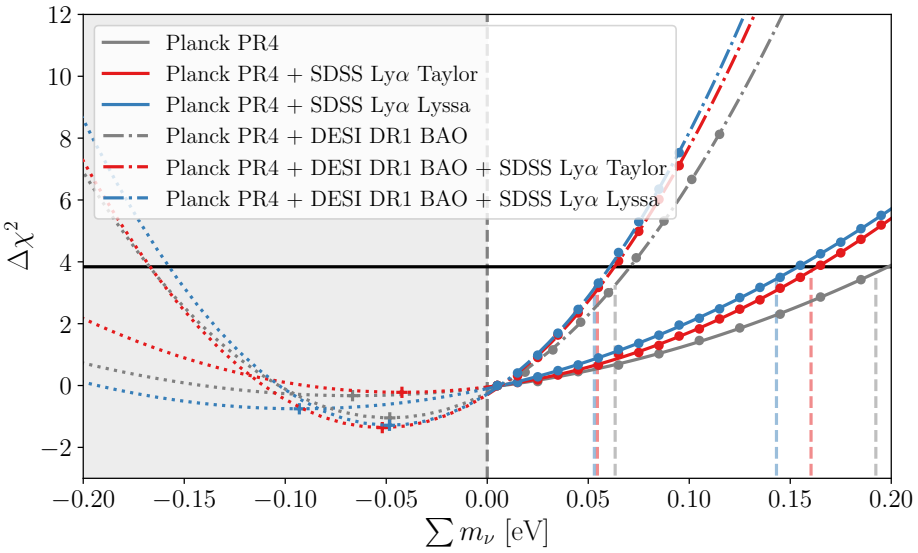

Figure 5. Profile likelihoods for combinations of CMB information from *Planck* PR4, BAO from DESI DR1 and Lyman-α likelihoods [87, 88]. Both Lyman-α likelihoods produce similar results, especially when combined with DESI BAO. The addition of Lyman-α consistently improves the constraining power.

JCAP01(2026)041

Lyssa. Constraints on $n_{\rm Lya}$ and $A_{\rm Lya}$ are of the same order or weaker than the ones obtained from *Planck*, so while it was not likely that introducing the Lyman-α information would constitute a huge improvement, nevertheless a shift in the limit was observed.

Although both Lyman-α likelihoods are based on the same eBOSS data, as noted in [88], the differences in simulations and methodology lead to different results. Typically, the authors find Lyssa $n_{\rm Lya}$ and Taylor $A_{\rm Lya}$ agree well with *Planck*, while the Lyssa $A_{\rm Lya}$ and Taylor $n_{\rm Lya}$ show some tension with *Planck*. The optimization performed for CMB + Lyman-α profiles show a similar trend.

We also combine *Planck* PR4 and Lyman-α likelihoods with DESI DR1 BAO, to compare the profiles to the combination of *Planck* PR4, DESI DR1 BAO and DESI DR1 full-shape from section 4.1.1. As for DESI full-shape, the upper limit is slightly pulled down by the addition of free-streaming information to the BAO+CMB combination, going from 63 meV to 55 and 53 meV for Taylor and Lyssa, respectively. However, unlike the case of the full-shape, for which the change in upper limit stemmed almost entirely from a shift of the parabola, the addition of Lyman-α introduces minimal shifts of the minimum. The change is driven by the tightening of σ, which decreases from 54 meV to 50 (Taylor) and 48 meV (Lyssa). Although the improvement remains small compared to the constraining power without the Lyman-α information, one can expect significant improvement from the upcoming P1D analysis of DESI data.

4.2 Extensions beyond flat ΛCDM

As previous analyses have noted, neutrino mass constraints exhibit an important model dependence [102]. In the following, we explore two extensions to the flat ΛCDM model that was used in section 4.1: dynamical dark energy, and non-zero curvature.

Although the introduction of a cosmological constant Λ continues to be the standard for cosmological analysis, recent data have sparked strong interest in the possibility of dynamical dark energy [34, 103–105]. It is commonly modeled by introducing the CPL parametrization of the equation of state of dark energy (section 3) and the modified model is referred to as $w_0w_{\rm a}$CDM. The combination of the most recent observations of the BAO feature, the CMB and Type Ia supernovae show that tensions between datasets are alleviated in $w_0w_{\rm a}$CDM, leading to a preference over ΛCDM [34]. The same data, when used for Bayesian inference in the determination of the neutrino mass, yield one-dimensional posteriors that peak at positive values.

Here, we investigate the effect of dynamical dark energy on the more stringent DESI DR2 BAO + CMB combinations of the previous section. Since $w_0w_{\rm a}$CDM introduces new degeneracies in the analysis, we expect the resulting constraint to be weakened. The introduction of data from Type Ia SN partially mitigates this loss of constraining power. Figure 6 presents the corresponding profile likelihoods. The most glaring difference with ΛCDM is that both DESI DR2 BAO + *Planck* PR4 and DESI DR2 BAO + ACT-lite now exhibit a minimum at positive values, at 24 and 41 meV respectively. This effect was also observed in [53]. As a consequence, the upper limit from the Feldman-Cousins prescription now coincides with $\Delta\chi^2 = 3.84$. Opening up the dark energy model to $w_0w_{\rm a}$CDM largely relaxes the constraints compared to ΛCDM. Although the parabolic fit is worse in $w_0w_{\rm a}$CDM,

JCAP01(2026)041

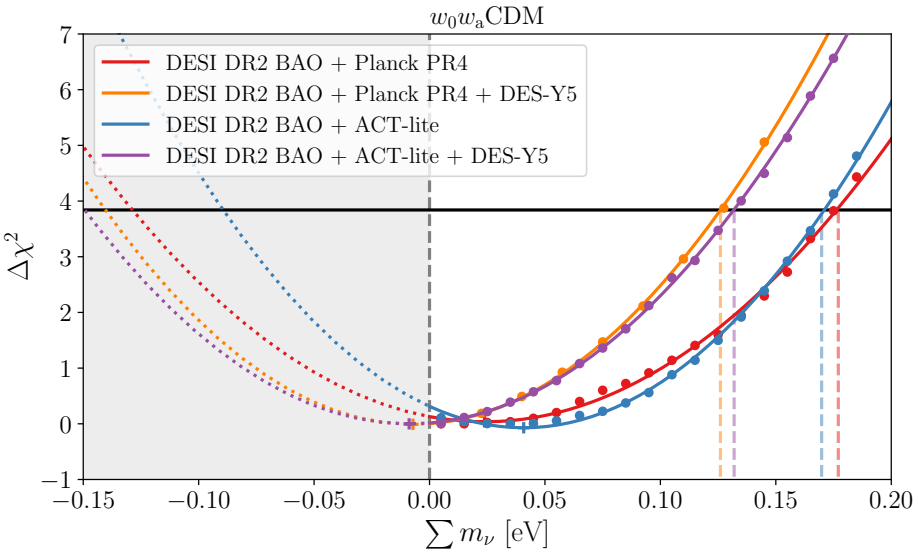

Figure 6. Profile likelihoods for combinations of BAO data, CMB data from *Planck* PR4 and SN from DES-Y5, in a w_0w_aCDM cosmological model. DESI DR2 BAO + CMB profiles now exhibit a minimum at a positive value. Adding SN information stabilizes both profiles in the same location, but the minimum moves back to a negative value.

we note that σ goes from 43 to about 78 meV for the DESI DR2 BAO + *Planck* PR4 combination. This broadening, as well as the shift of the minima, both contribute to the relaxation of the upper limit to $\sum m_\nu \leq 177$ meV. The inclusion of SN data from DES-Y5 pushes the minima slightly to a negative value and stabilizes both curves in the same location. The ACT-lite combination shows slightly looser constraining power than the *Planck* PR4 one. This situation is fully analogous to that presented in ΛCDM (section 4.1.1).

Our base ΛCDM model assumes flat spacetime. This hypothesis is commonly assumed in modern cosmological analyses and is supported by observation [33]. Simple inflation models lead to zero curvature, and measurements of Ω_K by the CMB alone or combined with BAO are consistent with a flat universe [34, 36, 58, 106]. These measurements are generally carried out at fixed neutrino mass; however, Ω_K is degenerate with $\sum m_\nu$, in particular through the geometrical effect used to determine the neutrino mass. Analyses conducted with free curvature, thus, find relaxed constraints for BAO and CMB combinations. In [107], the authors perform Bayesian inference and the recovered limits become compatible with the inverted ordering minimal mass again. In figure 7, we allow non-zero curvature by letting the parameter Ω_K be free.

As Ω_K can play a similar role to that of the neutrino mass in the geometrical effect, allowing non-zero curvature should decrease the constraining power of the data. Indeed, for the combination of DESI DR2 BAO and *Planck* PR4, varying the curvature degrades σ from 43 meV to 64 meV. The upper limit increases to 85 meV, which is high enough to permit normal hierarchy, however, the minimum moves further into the negative.

Indeed, DESI DR2 BAO + *Planck* PR4 favors positive Ω_K and only marginally higher Ω_m than flat ΛCDM [34]. As a consequence, it also should prefer even lower neutrino mass

JCAP01(2026)041

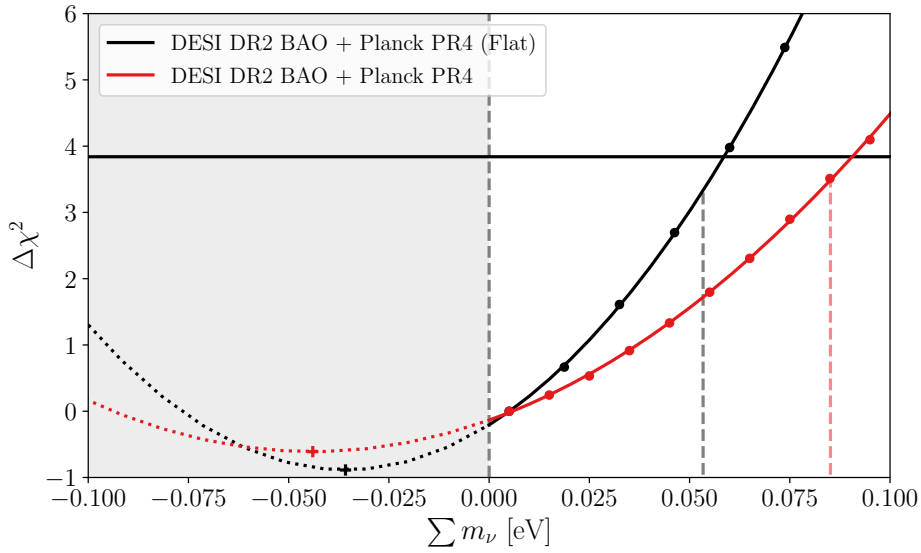

Figure 7. Profile likelihoods for DESI DR2 BAO + *Planck* PR4 in flat and non-flat ΛCDM cosmological models.

to compensate for the increase in Ω_K. This preference does not appear in the upper limit determination due to the degeneracy on the geometrical effect weakening the constraint, but it is visible in the overall shift of the profile.

The fit neutrino parameters are summarized in table 2.

5 Small-scale suppression with large-scale structures

In section 4, the constraint on neutrino mass is driven by a combination of geometrical information from the DESI BAO data and the *Planck* CMB observations, as well as measurements of the impact of neutrino free-streaming through CMB lensing measurements by *Planck* and ACT. When including full-shape information from DESI on top of BAO information, there is no significant improvement, which suggests that free-streaming constraints from CMB lensing information dominate the free-streaming constraints from large-scale structure measurements. It is important to investigate whether tight neutrino mass bounds can only be obtained using CMB information, or whether other data combinations can achieve constraints as well. In this section, we aim to derive constraints using as little free-streaming information from CMB as possible.

Since the high-ℓ polarization and temperature spectra of the CMB are still sensitive to the lensing effect, we do not use the full CMB information and compress the data to the slope and amplitude of the primordial power spectrum. We start from the DESI DR1 full-shape + BAO likelihood, and add information on $\Omega_b h^2$ from BBN as well as the CMB slope and amplitude description. The latter can be obtained from the *Planck* dataset by introducing its constraints on n_s and A_s, or by considering the quantities $n_{\rm Lya}$ and $A_{\rm Lya}$ from the simulation grids of the Lyman-α forest 1D power spectrum. In the ΛCDM framework, these approaches should be equivalent.

JCAP01(2026)041

	μ_0	σ	μ_{95}
ΛCDM			
DESI DR1 BAO + Planck PR4 (no lensing)	-0.068	0.067	0.074
DESI DR1 BAO + Planck PR4	-0.048	0.054	0.063
DESI DR2 BAO + Planck PR4	-0.036	0.043	0.053
DESI DR2 BAO + ACT-lite	-0.038	0.048	0.060
DESI DR1 BAO + Planck PR3 `plik`	-0.046	0.055	0.068
DESI DR1 FS+BAO + Planck PR3 `plik`	-0.063	0.053	0.053
Planck PR4	-0.067	0.130	0.192
Planck PR4 + SDSS Lyman-α Taylor	-0.042	0.102	0.160
Planck PR4 + SDSS Lyman-α Lyssa	-0.093	0.115	0.143
Planck PR4 + SDSS Lyman-α Taylor + DESI DR1 BAO	-0.052	0.050	0.055
Planck PR4 + SDSS Lyman-α Lyssa + DESI DR1 BAO	-0.048	0.048	0.053
w_0w_aCDM			
DESI DR2 BAO + Planck PR4	0.024	0.078	0.177
DESI DR2 BAO + Planck PR4 + DES-Y5	-0.007	0.068	0.126
DESI DR2 BAO + ACT-lite	0.041	0.066	0.171
DESI DR2 BAO + ACT-lite + DES-Y5	-0.009	0.077	0.132
Ω_K + ΛCDM			
DESI DR2 BAO + Planck PR4	-0.044	0.064	0.085

Table 2. Parabolic fits and derived parameters for data combinations in section 4. Parameters are reported in eV. Unless specified otherwise, CMB data includes CMB lensing.

5.1 Constraints on $\sum m_\nu$ with compressed primordial information from the CMB

Figure 8 presents the profiles for combinations of DESI full-shape and *Planck* information on the primordial power spectrum. We expect the switch from a loosened constraint on n_s to the original *Planck* one, and then the inclusion of A_s to improve the constraining power of the data combination.

The fit parameters reported in table 3 indeed show that σ improves by about 20 meV each time, going from 203 to 184 and then 163 meV. We also observe a strong decrease of the upper limit, by about 75 meV. The tightening of the parabola alone only contributes to about half of this shift; the rest is caused by the displacement of the parabola minimum toward the negative. Although important, especially after the inclusion of A_s, this shift leaves the profiles in reasonable tension with $\sum m_\nu \geq 0$, at $\chi^2_0 \sim 0.5$ at most.

Compared to the ΛCDM constraints given by the combination of BAO and CMB data, both constraining power and upper limits are greatly relaxed here. Several factors are at

JCAP01(2026)041

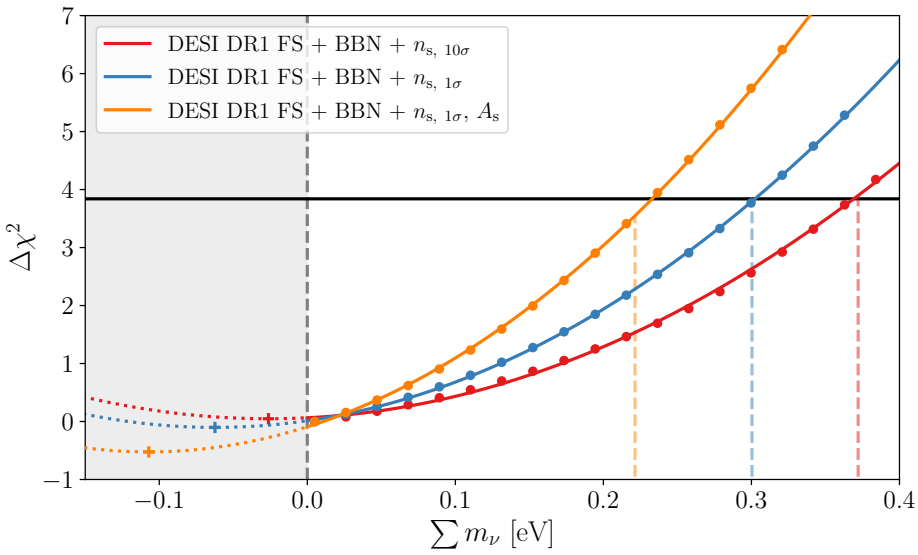

Figure 8. Combination of DESI full-shape (FS), BBN, and *Planck* information on n_s and A_s. Adding more constraining information from *Planck* drives a more stringent upper limit, but also tips the curves to negative values. The width of the parabolas σ also steadily decreases, which also contributes to the lowering of the upper limit.

play in this relaxation, and can be broken down in two categories depending on the neutrino mass effect — geometrical or free-streaming — that they affect.

First and foremost, the data combination does not include the CMB lensing measurement of small-scale suppression, which we determined in section 4.1.1 to be much more constraining than DESI full-shape. In the case in where the CMB lensing likelihood was not included, the constraining power in section 4.1.1 was about three times stronger. This is partly because, as mentioned above, even without including the lensing in the likelihood, the CMB spectra are sensitive to the lensing at small angular scales and, thus, to the free-streaming effect. Planck PR4 without the lensing is able to set a 68% C.L. upper limit at $\sum m_\nu < 0.161\,\text{eV}$ [58], which is of the same order as the 68% C.L. confidence limit of the loosest profile in figure 8. When reducing the information to n_s and A_s, this sensitivity is severely limited.

The remaining difference lies in disappearance of the geometrical effect. Although the DESI full-shape likelihood includes the BAO measurement, since we do not include the full CMB data in this section, there is essentially no geometrical constraint that comes into play, as highlighted in figure 1 of [53].

Unlike results from section 4, the profiles in figure 8 exhibit constraints on the neutrino mass that are based on DESI free-streaming measurements. Although the bounds are very relaxed compared to those obtained through leveraging of the CMB free-streaming measurement or the geometrical effect, they are fully compatible with these same results. Upcoming data releases should tighten the constraint. They will constitute another independent tool to constrain the neutrino mass, to be checked against those derived through other effects and probes.

JCAP01(2026)041

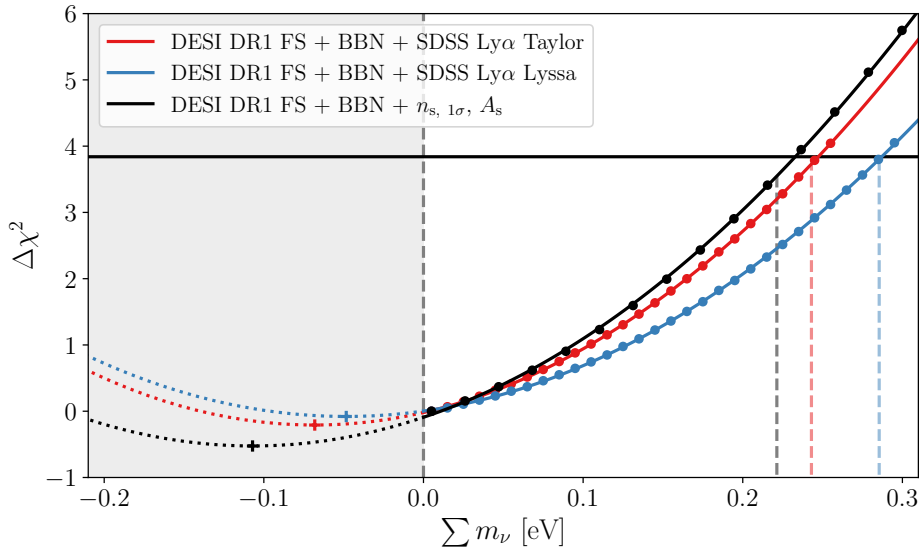

Figure 9. Combination of DESI full-shape (FS), BBN, and Lyman-α likelihoods from either the Taylor (red) or Lyssa (blue) simulation grids. All combinations result in comparable minimum positions. The Taylor-based profile is more constraining than the Lyssa one. The combination with *Planck* n_s and A_s from section 5.1 (black) is included for comparison.

5.2 Constraints on $\sum m_\nu$ with compressed primordial information from the Lyman-α forest

Although we successfully constrain the neutrino mass in section 5.1 using only the free-streaming effect measured by DESI, the constraint still relies on CMB information for the shape of the primordial power spectrum. In this section, our goal is to obtain bounds using exclusively large-scale structure probes. In order to do so, we drop the compressed CMB information and instead introduce the parameters $n_{\rm Lya}$, $A_{\rm Lya}$ of the Lyman-α P1D of eBOSS quasars.

In figure 9, we present profiles for combinations of DESI full-shape with BBN and several Lyman-α likelihoods. The corresponding fit parameters are reported in table 3. The cosmological parameter basis used in the Taylor and Lyssa analyses [87, 88] is composed of $\Omega_{\rm m}$ and H_0 in addition to $n_{\rm Lya}$ and $A_{\rm Lya}$. The Lyman-α likelihoods do not provide significant constraints on $\Omega_{\rm m}$ and H_0, especially compared to the other likelihoods included in the analysis. In addition, both of these parameters are almost uncorrelated to $n_{\rm Lya}$ and $A_{\rm Lya}$.[7] For these reasons, we remove them from the analysis, and expect this should not strongly impact the constraint.

The Taylor profile shown in figure 9 is more constraining than its Lyssa counterpart. Since both likelihoods are based on the data release 14 of SDSS, this is only attributable to a difference in modeling; either to the inclusion of a prior on H_0 in Taylor, or to the emulation differences discussed in the Lyssa publication [88].

The constraining powers σ of the combinations with either n_s and A_s from *Planck*, 163 meV, or $n_{\rm Lya}$ and $A_{\rm Lya}$ from the Lyman-α forest are comparable: 169 meV and 157 meV

[7] For Lyssa: around 3% correlation at most, except for $\Omega_{\rm m}$ and $n_{\rm Lya}$ at about 20%.

JCAP01(2026)041

	μ_0	σ	μ_{95}
DESI FS + BBN + $n_{\mathrm{s},\ 10\sigma}$	-0.026	0.203	0.372
DESI FS + BBN + $n_{\mathrm{s},\ 1\sigma}$	-0.062	0.184	0.300
DESI FS + BBN + $n_{\mathrm{s},\ 1\sigma}$, A_s	-0.107	0.163	0.221
DESI FS + BBN + SDSS Lyman-α Taylor	-0.068	0.157	0.243
DESI FS + BBN + SDSS Lyman-α Lyssa	-0.048	0.169	0.285

Table 3. Parabolic fit parameters for data combinations in section 5. Parameters are reported in eV.

with the Lyssa and Taylor likelihoods, respectively. Although the profile based on Lyman-α provides a less stringent upper limit, this is almost entirely attributable to a shift in the minimum position and not to a difference in statistical strength. Indeed, the *Planck*-based profile is shifted to the negative compared to Lyman-α. We expect that this shift is mostly driven by the difference in the spectral index constrained by each dataset; both Lyman-α likelihood combinations are minimized by lower values of n_{s} than the one constrained by *Planck*, which can be compensated by a higher neutrino mass.

As in section 5.1, the bounds we obtain with DESI free-streaming measurements are very relaxed compared to geometry with BAO or free-streaming with CMB lensing. Nevertheless, this particular combination of tracers successfully yields a constraint on the neutrino mass solely based on large-scale structures probes. The constrained effect is different from a geometry-based DESI BAO + CMB (no lensing) analysis, and the set of probes is completely separate from CMB free-streaming constraints. The fact that independent constraints at our disposal agree with each other constitutes an important coherence check.

6 Individual neutrino masses

6.1 Mass splitting model

All profile likelihoods presented in previous sections are computed under the so-called degenerate mass assumption, in which there are three massive neutrinos such that

$$m_1 = m_2 = m_3 = \frac{1}{3}\sum m_\nu. \tag{6.1}$$

Although we know from oscillation experiments that this hypothesis is not true, it is a standard way of modeling the mass splitting. It has been shown to be a reasonable approximation for cosmological determination of the neutrino mass [26, 27, 108, 109], and is the one assumed in recent major data releases and their neutrino analysis, although they also considered mass splittings [34, 53, 99]. Other notable approaches include the one originally taken in the *Planck* data releases, which report results in ΛCDM with a fixed total mass $\sum m_\nu = 0.059\,\mathrm{eV}$ made up of one massive neutrino only, and set the two other particles to be massless. This approach continues to be taken in current major data releases such as [34, 36, 38].

Compared to the mass splitting dictated by the normal or inverted ordering, the degenerate approximation breaks down when the total mass approaches the boundaries set by either scheme. In this region, the lightest neutrino mass m_{l} becomes much smaller than the heaviest

JCAP01(2026)041

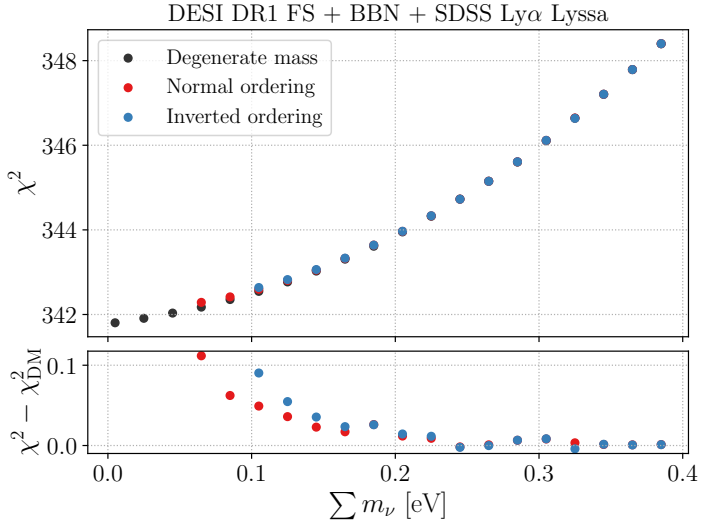

Figure 10. Non-normalized profile likelihoods for DESI full-shape, BBN and information on $n_{\rm Lya}$, $A_{\rm Lya}$ from the Lyssa likelihood, for different mass splitting modelings in `CAMB`.

one, however, cosmological data is primarily influenced by the total mass $\sum m_\nu$, which does not depend on the modeling. In this section, we endeavor to study how big of an impact the modeling choice can have on cosmological analyses.

As briefly discussed in section 1, cosmology is almost insensitive to the individual neutrino masses. They mostly affect the non-relativistic transition redshift z_ν, since heavier neutrinos transition earlier. Keeping in mind that $z_\nu = m_\nu/(53 \times 10^{-5}\,\text{eV}) - 1$ [25], we are assured that at least two of the three species have completed their non-relativistic transition between recombination and recent times, and are participating in the gravitational effects described in section 1. Heavier neutrinos can start affecting clustering and contributing to $\rho_{\rm m}(z)$ earlier, however, which modifies the small-scale suppression effect. The free-streaming scale $\lambda_{\rm fs}$ also technically depends on the individual neutrino masses, further affecting the small scales of the matter power spectrum. In order to gauge whether the degenerate mass assumption is still valid, we compute a profile likelihood for a given set of information and varied the mass splitting model in the Boltzmann solver, `CAMB`. The results are presented in figure 10.

As expected, the biggest variation between modelings happens very close to the respective boundaries of the orderings. There, the difference in χ^2 compared to a degenerate mass modeling reaches 0.11. Generally speaking, the degenerate mass assumption leads to a slight overestimation of the maximized likelihood close to the ordering boundaries. As a consequence, the minima of the profiles shift towards positive values, and the parabolas close up slightly. The effect on σ is limited, however, with variations of 8% at most, as visible in table 4 where we report parabola parameters and the associated upper limits. Similar orders of variation were observed for other likelihood combinations of comparable constraining power, such as the combination of DESI full-shape and *Planck* measurements of the primordial power spectrum. For such data combinations, the degenerate mass modeling exhibits reasonable differences with the inverted and normal modelings. The effect on the conclusions of the analysis, especially the upper limit $\mu_{95}^{(\rm IO)}$ or $\mu_{95}^{(\rm NO)}$, remain constrained to a few percents.

JCAP01(2026)041

	μ_0	σ	μ_{95}	μ_0	σ	$\mu_{95}^{(\mathrm{NO})}$	μ_0	σ	$\mu_{95}^{(\mathrm{IO})}$
Degenerate	-0.049	0.170	0.285	-0.042	0.167	0.294	-0.039	0.166	0.302
Normal	—	—	—	-0.019	0.160	0.299	-0.022	0.161	0.306
Inverted	—	—	—	—	—	—	-0.010	0.157	0.309

Table 4. Parabolic fit parameters for DESI full-shape, BBN and information on n_{Lya}, A_{Lya} from the Lyssa likelihood with different mass splitting models in `CAMB`, as plotted in figure 10. Parameters are reported in eV.

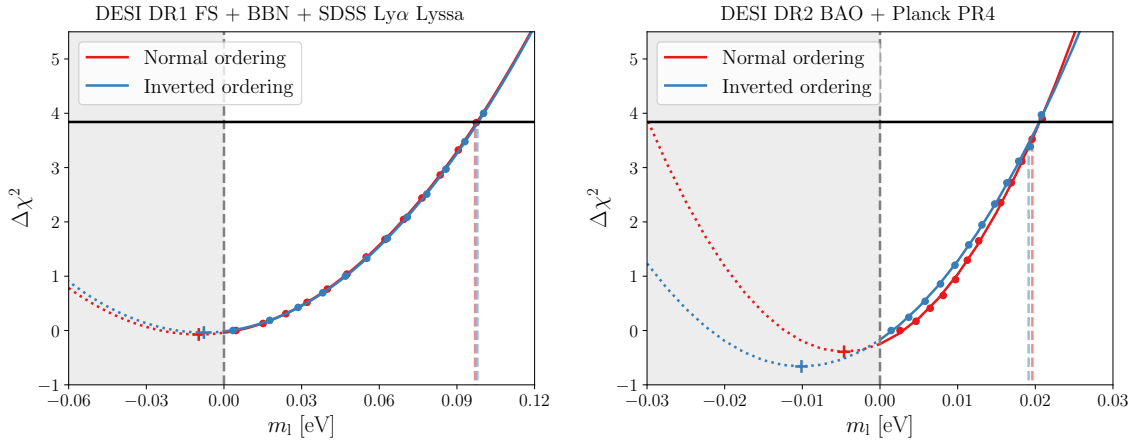

(a) DESI full-shape, BBN, Lyman-α.

(b) DESI DR2 BAO, *Planck* PR4.

Figure 11. Profile likelihoods for the lightest neutrino mass m_l based on two likelihood combinations: either DESI full-shape, BBN and Lyssa, or the most constraining DESI DR2 BAO and *Planck* PR4.

On the other hand, for more constraining data combinations, such a test is not suitable anymore, for several reasons. Indeed, profiles such as those featured in section 4 result in 95% C.L. limits below the inverted ordering limit, and even below the normal ordering limit in some cases. Consequently, there is no doubt that comparable results cannot be obtained with the inverted or normal modeling. Additionally, it is not conceivable to produce a profile from such constraining data combinations, all the while requiring $\sum m_\nu \geq 59\,\mathrm{meV}$ or $100\,\mathrm{meV}$. Since such masses are very distant from the parabola's minimum, the analysis would be limited to a region where the parabolic fit cannot be expected to hold up.

6.2 Lightest neutrino mass

When working with neutrino mass in cosmology, $\sum m_\nu$ is a natural parameter choice as it is more directly constrained. However, for a given modeling of the mass splitting, which informs us on mass differences, the constraint on $\sum m_\nu$ may be equivalently translated to one on the mass of the lightest neutrino. For the normal ordering, the lightest neutrino has mass m_1, while in the inverted ordering, its mass is m_3. We refer to the lightest mass indifferently as m_l. Translated results for two likelihood combinations are presented on figure 11.

In the case of the more relaxed combination which involves DESI full-shape, BBN and Lyssa Lyman-α, in both normal and inverted ordering, the minimum of the parabola is at a

JCAP01(2026)041

	μ_0	σ	μ_{95}
DESI full-shape + BBN + Lyssa $n_{\rm Lya}$, $A_{\rm Lya}$			
Normal ordering	-0.009	0.054	0.097
Inverted ordering	-0.007	0.053	0.098
DESI DR2 BAO + Planck PR4			
Normal ordering	-0.005	0.012	0.020
Inverted ordering	-0.010	0.014	0.019

Table 5. Parabolic fit parameters for the lightest neutrino mass profiles of figure 11. Parameters are reported in eV.

negative value, and the constraints are very close. This behavior is consistent with the previous $\sum m_\nu$ profiles, which preferred a total mass as small as possible. The similarity of the profiles is owed to the similarity of the normal and inverted ordering profiles in figure 10. The ranges $m_{\rm l} \in [0, \mu_{95}]$ correspond to $\sum m_\nu \in [0.059\,{\rm eV}, 0.305\,{\rm eV}]$ and $\sum m_\nu \in [0.100\,{\rm eV}, 0.320\,{\rm eV}]$, so there is important overlap in a region where the χ^2 values are very similar. The 95% upper limits derived from the profiles, for DESI full-shape, BBN and the Lyman-α Lyssa likelihood on $n_{\rm Lya}$ and $A_{\rm Lya}$ are

$$\begin{aligned} m_{\rm l} &< 0.097\,{\rm eV} \quad (95\%,\ \text{Normal ordering}) \\ m_{\rm l} &< 0.098\,{\rm eV} \quad (95\%,\ \text{Inverted ordering}). \end{aligned} \tag{6.2}$$

When applying the same process to the most constraining combination of DESI DR2 BAO and *Planck* PR4, although the upper limits are once again very similar, the profiles themselves differ. Indeed, due to the tightness of the constraint, $m_{\rm l}$ evolves in a domain where the corresponding $\sum m_\nu$ ranges in normal and inverted ordering do not overlap: approximately $[0.059\,{\rm eV}, 0.095\,{\rm eV}]$ and $[0.100\,{\rm eV}, 0.130\,{\rm eV}]$. The minima are once again at negative values, consistently with the preference for masses below the ordering minima. The 95% upper limits from DESI DR2 BAO and *Planck* PR4 are

$$\begin{aligned} m_{\rm l} &< 0.020\,{\rm eV} \quad (95\%,\ \text{Normal ordering}) \\ m_{\rm l} &< 0.019\,{\rm eV} \quad (95\%,\ \text{Inverted ordering}). \end{aligned} \tag{6.3}$$

These results are in agreement with the similar analysis carried out in the Bayesian formalism in [53], which found 95% credible limits at 23 and 24 meV respectively for the same data combination.

7 Conclusion

With recent cosmological data releases, the upper bound on the sum of neutrino masses $\sum m_\nu$ is steadily decreasing. Combination of major probes such as BAO, CMB, and CMB lensing now produce credible intervals that exclude the minimal mass imposed by the inverted ordering, and continue to creep closer to the normal hierarchy bound of 59 meV. The interpretation of these upper bounds is complicated by the proximity to the physical bound at $\sum m_\nu = 0$.

JCAP01(2026)041

Furthermore, the development of EFT-based likelihoods such as DESI full-shape and the rising interest in alternatives to ΛCDM has caused the investigated parameter spaces to expand greatly, leading to legitimate concern that volume effects may affect Bayesian analyses.

In this work, we have approached the problem from a frequentist point of view, and chosen to construct profile likelihoods for the neutrino mass. Such an approach is devoid of any prior and volume effects, and independent of the choice of cosmological basis. The closeness of the zero mass bound can be accounted for in the confidence limit by applying the Feldman-Cousins prescription [57]. Additionally, profiles of Gaussian likelihood take the shape of a parabola, whose parameters can be fit and used to determine the constraining power σ of the profiled data separately from the confidence limit. This constitutes a powerful tool in the comparison of different datasets.

We find that in a base ΛCDM+$\sum m_\nu$ cosmological model, using a variety of dataset combinations, all profiles are cut off by the zero mass bound, and the corresponding parabolas reach their minima at unphysical mass ($\sum m_\nu < 0$).

We first investigate classic data combinations of BAO and CMB data, wherein the bulk of the constraint comes from the geometrical effect of the neutrino mass, with a free-streaming contribution from CMB lensing. The most stringent data combination, made up of DESI DR2 BAO, CMB from *Planck* PR4, and CMB lensing from ACT DR6 and *Planck* PR4, yields a 95% C.L. limit of 53 meV, which falls below both normal and inverted ordering minima. Changes in the CMB likelihood, such as considering *Planck* PR3 or ACT DR6, leave the profiles mostly unaffected aside from a slight loosening. By contrast, the addition of free-streaming measurements by the DESI DR1 full-shape analysis highlights the distinction between the confidence limit and the constraining power σ. Indeed, the confidence limit is artificially pulled down by the shift of the whole parabola, even though the constraining power shows limited gain. Free-streaming information can also be found in the Lyman-α P1D. Actually, despite currently stemming from SDSS data, the Lyman-α likelihood already shows interesting added value on σ, comparable to or even exceeding that of DESI full-shape.

The determination of the neutrino mass through cosmological means is inherently model dependent. We consider two extensions to the ΛCDM model: non-zero spatial curvature and dynamical dark energy. These extensions have long been studied and have recently seen renewed interest, especially in the context of the neutrino mass [53, 107]. Overall, constraints in such extensions are very relaxed by new degeneracies, and all confidence limits now allow at least the normal ordering. Only w_0w_aCDM shows a migration of the profiles in the direction of physical mass ($\sum m_\nu \geq 0$), even exhibiting a trough firmly at positive values in some cases.

Additionally, we considered novel data combinations to derive neutrino mass constraints that rely on free-streaming measurement by large scale structure probes exclusively. This is made possible by combining the DESI full-shape and BAO information to BBN data and Lyman-α P1D measurements. We find that we are able to constrain the neutrino mass independently of the CMB to $\sum m_\nu \leq 0.243$ eV and $\sum m_\nu \leq 0.285$ eV, depending on the Lyman-α implementation we use. Such data combinations still present an extrapolated minimum at negative values. They can be put into perspective by considering CMB-only (without lensing) constraints, that stand at 0.36 and 0.39 eV for *Planck* PR4 data [56, 58].

JCAP01(2026)041

Finally, we applied the same formalism to compute profile likelihoods of $m_{\rm l}$, the lightest neutrino mass. This computation becomes ordering dependent, although both orderings yield similar results. In particular, for DESI DR2 BAO and *Planck* PR4 in ΛCDM, we find limits at 20 and 19 meV in the normal and inverted ordering.

Overall, the minima of the profiles most often lie below zero. While $w_0w_{\rm a}$CDM constitutes an interesting exception to this trend, we note that the tensions with physical mass ($\sum m_\nu \geq 0$) remain very limited in the ΛCDM cosmological model, rarely exceeding $\chi^2_0 = 1$. This highlights the need for continued research in this area. Future neutrino mass analyses will especially benefit from upcoming DESI data, including DR1 Lyman-α, DR2 full-shape and DR3 BAO.

Data availability. The DESI data used in this analysis will be made public along the Data Release 2 (details in https://data.desi.lbl.gov/doc/releases/). The data needed to reproduce all figures in this paper are available on Zenodo: https://doi.org/10.5281/zenodo.15878410.

Acknowledgments

DC, CY and EA acknowledge support from the ANR grant ANR-22-CE92-0037. MW acknowledges support by the project AIM@LMU funded by the German Federal Ministry of Education and Research (BMBF) under the grant number 16DHBKI013. MW acknowledges support from the Excellence Cluster ORIGINS which is funded by the Deutsche Forschungsgemeinschaft (DFG, German Research Foundation) under Germany's Excellence Strategy — EXC-2094 — 390783311. JR acknowledges funding from US Department of Energy grant DE-SC0016021.

This material is based upon work supported by the U.S. Department of Energy (DOE), Office of Science, Office of High-Energy Physics, under Contract No. DE-AC02-05CH11231, and by the National Energy Research Scientific Computing Center, a DOE Office of Science User Facility under the same contract. Additional support for DESI was provided by the U.S. National Science Foundation (NSF), Division of Astronomical Sciences under Contract No. AST-0950945 to the NSF's National Optical-Infrared Astronomy Research Laboratory; the Science and Technology Facilities Council of the United Kingdom; the Gordon and Betty Moore Foundation; the Heising-Simons Foundation; the French Alternative Energies and Atomic Energy Commission (CEA); the National Council of Humanities, Science and Technology of Mexico (CONAHCYT); the Ministry of Science, Innovation and Universities of Spain (MICIU/AEI/10.13039/501100011033), and by the DESI Member Institutions: https://www.desi.lbl.gov/collaborating-institutions. Any opinions, findings, and conclusions or recommendations expressed in this material are those of the author(s) and do not necessarily reflect the views of the U.S. National Science Foundation, the U.S. Department of Energy, or any of the listed funding agencies.

The authors are honored to be permitted to conduct scientific research on I'oligam Du'ag (Kitt Peak), a mountain with particular significance to the Tohono O'odham Nation.

JCAP01(2026)041

References

[1] R. Davis Jr., D.S. Harmer and K.C. Hoffman, *Search for neutrinos from the sun*, *Phys. Rev. Lett.* **20** (1968) 1205 [INSPIRE].

[2] J.N. Bahcall and R. Davis, *Solar neutrinos — a scientific puzzle*, *Science* **191** (1976) 264 [INSPIRE].

[3] GALLEX collaboration, *First results from the Cr-51 neutrino source experiment with the GALLEX detector*, *Phys. Lett. B* **342** (1995) 440 [INSPIRE].

[4] SAGE collaboration, *Results from SAGE*, *Phys. Lett. B* **328** (1994) 234 [INSPIRE].

[5] SUPER-KAMIOKANDE collaboration, *Measurements of the solar neutrino flux from Super-Kamiokande's first 300 days*, *Phys. Rev. Lett.* **81** (1998) 1158 [*Erratum ibid.* **81** (1998) 4279] [hep-ex/9805021] [INSPIRE].

[6] SNO collaboration, *Measurement of the rate of $\nu_e + d \to p + p + e^-$ interactions produced by ^8B solar neutrinos at the Sudbury Neutrino Observatory*, *Phys. Rev. Lett.* **87** (2001) 071301 [nucl-ex/0106015] [INSPIRE].

[7] BOREXINO collaboration, *Direct measurement of the Be-7 solar neutrino flux with 192 days of Borexino data*, *Phys. Rev. Lett.* **101** (2008) 091302 [arXiv:0805.3843] [INSPIRE].

[8] SUPER-KAMIOKANDE collaboration, *Evidence for oscillation of atmospheric neutrinos*, *Phys. Rev. Lett.* **81** (1998) 1562 [hep-ex/9807003] [INSPIRE].

[9] MACRO collaboration, *Matter effects in upward going muons and sterile neutrino oscillations*, *Phys. Lett. B* **517** (2001) 59 [hep-ex/0106049] [INSPIRE].

[10] SOUDAN 2 collaboration, *Measurement of the L/E distributions of atmospheric neutrinos in Soudan 2 and their interpretation as neutrino oscillations*, *Phys. Rev. D* **68** (2003) 113004 [hep-ex/0307069] [INSPIRE].

[11] ICECUBE collaboration, *Measurement of atmospheric tau neutrino appearance with IceCube DeepCore*, *Phys. Rev. D* **99** (2019) 032007 [arXiv:1901.05366] [INSPIRE].

[12] ANTARES collaboration, *Measuring the atmospheric neutrino oscillation parameters and constraining the 3+1 neutrino model with ten years of ANTARES data*, *JHEP* **06** (2019) 113 [arXiv:1812.08650] [INSPIRE].

[13] K2K collaboration, *Measurement of neutrino oscillation by the K2K experiment*, *Phys. Rev. D* **74** (2006) 072003 [hep-ex/0606032] [INSPIRE].

[14] MINOS collaboration, *Combined analysis of ν_μ disappearance and $\nu_\mu \to \nu_e$ appearance in MINOS using accelerator and atmospheric neutrinos*, *Phys. Rev. Lett.* **112** (2014) 191801 [arXiv:1403.0867] [INSPIRE].

[15] MINOS+ collaboration, *Precision constraints for three-flavor neutrino oscillations from the full MINOS+ and MINOS dataset*, *Phys. Rev. Lett.* **125** (2020) 131802 [arXiv:2006.15208] [INSPIRE].

[16] OPERA collaboration, *Final results of the OPERA experiment on ν_τ appearance in the CNGS neutrino beam*, *Phys. Rev. Lett.* **120** (2018) 211801 [*Erratum ibid.* **121** (2018) 139901] [arXiv:1804.04912] [INSPIRE].

[17] C. Rubbia et al., *Underground operation of the ICARUS T600 LAr-TPC: first results*, 2011 *JINST* **6** P07011 [arXiv:1106.0975] [INSPIRE].

JCAP01(2026)041

[18] T2K collaboration, *Indication of electron neutrino appearance from an accelerator-produced off-axis muon neutrino beam*, *Phys. Rev. Lett.* **107** (2011) 041801 [arXiv:1106.2822] [INSPIRE].

[19] NOvA collaboration, *Constraints on oscillation parameters from ν_e appearance and ν_μ disappearance in NOvA*, *Phys. Rev. Lett.* **118** (2017) 231801 [arXiv:1703.03328] [INSPIRE].

[20] KamLAND collaboration, *First results from KamLAND: evidence for reactor anti-neutrino disappearance*, *Phys. Rev. Lett.* **90** (2003) 021802 [hep-ex/0212021] [INSPIRE].

[21] Double Chooz collaboration, *Indication of reactor $\bar{\nu}_e$ disappearance in the Double Chooz experiment*, *Phys. Rev. Lett.* **108** (2012) 131801 [arXiv:1112.6353] [INSPIRE].

[22] Daya Bay collaboration, *Observation of electron-antineutrino disappearance at Daya Bay*, *Phys. Rev. Lett.* **108** (2012) 171803 [arXiv:1203.1669] [INSPIRE].

[23] RENO collaboration, *Observation of reactor electron antineutrino disappearance in the RENO experiment*, *Phys. Rev. Lett.* **108** (2012) 191802 [arXiv:1204.0626] [INSPIRE].

[24] JUNO collaboration, *JUNO physics and detector*, *Prog. Part. Nucl. Phys.* **123** (2022) 103927 [arXiv:2104.02565] [INSPIRE].

[25] Particle Data Group collaboration, *Review of particle physics*, *Phys. Rev. D* **110** (2024) 030001 [INSPIRE].

[26] J. Lesgourgues, S. Pastor and L. Perotto, *Probing neutrino masses with future galaxy redshift surveys*, *Phys. Rev. D* **70** (2004) 045016 [hep-ph/0403296] [INSPIRE].

[27] M. Archidiacono, S. Hannestad and J. Lesgourgues, *What will it take to measure individual neutrino mass states using cosmology?*, *JCAP* **09** (2020) 021 [arXiv:2003.03354] [INSPIRE].

[28] J. Lesgourgues and S. Pastor, *Massive neutrinos and cosmology*, *Phys. Rept.* **429** (2006) 307 [astro-ph/0603494] [INSPIRE].

[29] J. Lesgourgues and S. Pastor, *Neutrino mass from cosmology*, *Adv. High Energy Phys.* **2012** (2012) 608515 [arXiv:1212.6154] [INSPIRE].

[30] S. Hannestad, *Neutrino physics from precision cosmology*, *Prog. Part. Nucl. Phys.* **65** (2010) 185 [arXiv:1007.0658] [INSPIRE].

[31] DESI collaboration, *The DESI experiment, a whitepaper for Snowmass 2013*, arXiv:1308.0847 [INSPIRE].

[32] DESI collaboration, *The DESI experiment part II: instrument design*, arXiv:1611.00037 [INSPIRE].

[33] DESI collaboration, *DESI 2024 VI: cosmological constraints from the measurements of baryon acoustic oscillations*, *JCAP* **02** (2025) 021 [arXiv:2404.03002] [INSPIRE].

[34] DESI collaboration, *DESI DR2 results. II. Measurements of baryon acoustic oscillations and cosmological constraints*, *Phys. Rev. D* **112** (2025) 083515 [arXiv:2503.14738] [INSPIRE].

[35] Planck collaboration, *Planck 2018 results. V. CMB power spectra and likelihoods*, *Astron. Astrophys.* **641** (2020) A5 [arXiv:1907.12875] [INSPIRE].

[36] Planck collaboration, *Planck 2018 results. VI. Cosmological parameters*, *Astron. Astrophys.* **641** (2020) A6 [*Erratum ibid.* **652** (2021) C4] [arXiv:1807.06209] [INSPIRE].

[37] S. Roy Choudhury and S. Hannestad, *Updated results on neutrino mass and mass hierarchy from cosmology with Planck 2018 likelihoods*, *JCAP* **07** (2020) 037 [arXiv:1907.12598] [INSPIRE].

JCAP01(2026)041

[38] Atacama Cosmology Telescope collaboration, *The Atacama Cosmology Telescope: DR6 power spectra, likelihoods and ΛCDM parameters*, *JCAP* **11** (2025) 062 [arXiv:2503.14452] [INSPIRE].

[39] A.G. Doroshkevich, Y.B. Zeldovich, R.A. Sunyaev and M. Khlopov, *Astrophysical implications of the neutrino rest mass. II. The density-perturbation spectrum and small-scale fluctuations in the microwave background*, *Sov. Astron. Lett.* **6** (1980) 252 [INSPIRE].

[40] W. Hu, D.J. Eisenstein and M. Tegmark, *Weighing neutrinos with galaxy surveys*, *Phys. Rev. Lett.* **80** (1998) 5255 [astro-ph/9712057] [INSPIRE].

[41] A. Kiakotou, O. Elgaroy and O. Lahav, *Neutrino mass, dark energy, and the linear growth factor*, *Phys. Rev. D* **77** (2008) 063005 [arXiv:0709.0253] [INSPIRE].

[42] DESI collaboration, *DESI 2024 VII: cosmological constraints from the full-shape modeling of clustering measurements*, *JCAP* **07** (2025) 028 [arXiv:2411.12022] [INSPIRE].

[43] M.M. Ivanov, M. Simonović and M. Zaldarriaga, *Cosmological parameters and neutrino masses from the final Planck and full-shape BOSS data*, *Phys. Rev. D* **101** (2020) 083504 [arXiv:1912.08208] [INSPIRE].

[44] J. Lesgourgues, L. Perotto, S. Pastor and M. Piat, *Probing neutrino masses with CMB lensing extraction*, *Phys. Rev. D* **73** (2006) 045021 [astro-ph/0511735] [INSPIRE].

[45] ACT collaboration, *The Atacama Cosmology Telescope: DR6 gravitational lensing map and cosmological parameters*, *Astrophys. J.* **962** (2024) 113 [arXiv:2304.05203] [INSPIRE].

[46] ACT collaboration, *The Atacama Cosmology Telescope: a measurement of the DR6 CMB lensing power spectrum and its implications for structure growth*, *Astrophys. J.* **962** (2024) 112 [arXiv:2304.05202] [INSPIRE].

[47] Planck collaboration, *Planck 2018 results. VIII. Gravitational lensing*, *Astron. Astrophys.* **641** (2020) A8 [arXiv:1807.06210] [INSPIRE].

[48] J. Carron, M. Mirmelstein and A. Lewis, *CMB lensing from Planck PR4 maps*, *JCAP* **09** (2022) 039 [arXiv:2206.07773] [INSPIRE].

[49] L. Herold, E.G.M. Ferreira and L. Heinrich, *Profile likelihoods in cosmology: when, why, and how illustrated with ΛCDM, massive neutrinos, and dark energy*, *Phys. Rev. D* **111** (2025) 083504 [arXiv:2408.07700] [INSPIRE].

[50] N. Craig, D. Green, J. Meyers and S. Rajendran, *No νs is good news*, *JHEP* **09** (2024) 097 [arXiv:2405.00836] [INSPIRE].

[51] D. Green and J. Meyers, *Cosmological preference for a negative neutrino mass*, *Phys. Rev. D* **111** (2025) 083507 [arXiv:2407.07878] [INSPIRE].

[52] W. Elbers et al., *Negative neutrino masses as a mirage of dark energy*, *Phys. Rev. D* **111** (2025) 063534 [arXiv:2407.10965] [INSPIRE].

[53] W. Elbers et al., *Constraints on neutrino physics from DESI DR2 BAO and DR1 full shape*, *Phys. Rev. D* **112** (2025) 083513 [arXiv:2503.14744] [INSPIRE].

[54] Planck collaboration, *Planck intermediate results. XVI. Profile likelihoods for cosmological parameters*, *Astron. Astrophys.* **566** (2014) A54 [arXiv:1311.1657] [INSPIRE].

[55] D. Naredo-Tuero et al., *Critical look at the cosmological neutrino mass bound*, *Phys. Rev. D* **110** (2024) 123537 [arXiv:2407.13831] [INSPIRE].

[56] M. Tristram et al., *Cosmological parameters derived from the final Planck data release (PR4)*, *Astron. Astrophys.* **682** (2024) A37 [arXiv:2309.10034] [INSPIRE].

JCAP01(2026)041

[57] G.J. Feldman and R.D. Cousins, *A unified approach to the classical statistical analysis of small signals*, *Phys. Rev. D* **57** (1998) 3873 [physics/9711021] [INSPIRE].

[58] E. Rosenberg, S. Gratton and G. Efstathiou, *CMB power spectra and cosmological parameters from Planck PR4 with CamSpec*, *Mon. Not. Roy. Astron. Soc.* **517** (2022) 4620 [arXiv:2205.10869] [INSPIRE].

[59] L. Pagano et al., *Reionization optical depth determination from Planck HFI data with ten percent accuracy*, *Astron. Astrophys.* **635** (2020) A99 [arXiv:1908.09856] [INSPIRE].

[60] DESI collaboration, *Overview of the instrumentation for the Dark Energy Spectroscopic Instrument*, *Astron. J.* **164** (2022) 207 [arXiv:2205.10939] [INSPIRE].

[61] C. Poppett et al., *Overview of the fiber system for the Dark Energy Spectroscopic Instrument*, *Astron. J.* **168** (2024) 245.

[62] DESI collaboration, *The optical corrector for the Dark Energy Spectroscopic Instrument*, *Astron. J.* **168** (2024) 95 [arXiv:2306.06310] [INSPIRE].

[63] DESI collaboration, *The robotic multiobject focal plane system of the Dark Energy Spectroscopic Instrument (DESI)*, *Astron. J.* **165** (2023) 9 [arXiv:2205.09014] [INSPIRE].

[64] DESI collaboration, *Overview of the DESI legacy imaging surveys*, *Astron. J.* **157** (2019) 168 [arXiv:1804.08657] [INSPIRE].

[65] A.D. Myers et al., *The target-selection pipeline for the Dark Energy Spectroscopic Instrument*, *Astron. J.* **165** (2023) 50 [arXiv:2208.08518] [INSPIRE].

[66] DESI collaboration, *The spectroscopic data processing pipeline for the Dark Energy Spectroscopic Instrument*, *Astron. J.* **165** (2023) 144 [arXiv:2209.14482] [INSPIRE].

[67] DESI collaboration, *Performance of the quasar spectral templates for the Dark Energy Spectroscopic Instrument*, *Astron. J.* **166** (2023) 66 [arXiv:2305.10426] [INSPIRE].

[68] DESI collaboration, *Survey operations for the Dark Energy Spectroscopic Instrument*, *Astron. J.* **166** (2023) 259 [arXiv:2306.06309] [INSPIRE].

[69] T.-W. Lan et al., *The DESI survey validation: results from visual inspection of bright galaxies, luminous red galaxies, and emission-line galaxies*, *Astrophys. J.* **943** (2023) 68 [arXiv:2208.08516] [INSPIRE].

[70] D.M. Alexander et al., *The DESI survey validation: results from visual inspection of the quasar survey spectra*, *Astron. J.* **165** (2023) 124 [arXiv:2208.08517] [INSPIRE].

[71] A.P. Cooper et al., *Overview of the DESI Milky Way survey*, *Astrophys. J.* **947** (2023) 37 [arXiv:2208.08514] [INSPIRE].

[72] C.H. Hahn et al., *The DESI bright galaxy survey: final target selection, design, and validation*, *Astron. J.* **165** (2023) 253 [arXiv:2208.08512] [INSPIRE].

[73] S. Juneau et al., *Identifying missing quasars from the DESI bright galaxy survey*, *Astron. J.* **169** (2025) 157 [arXiv:2404.03621] [INSPIRE].

[74] DESI collaboration, *Target selection and validation of DESI luminous red galaxies*, *Astron. J.* **165** (2023) 58 [arXiv:2208.08515] [INSPIRE].

[75] A. Raichoor et al., *Target selection and validation of DESI emission line galaxies*, *Astron. J.* **165** (2023) 126 [arXiv:2208.08513] [INSPIRE].

[76] E. Chaussidon et al., *Target selection and validation of DESI quasars*, *Astrophys. J.* **944** (2023) 107 [arXiv:2208.08511] [INSPIRE].

JCAP01(2026)041

[77] DESI collaboration, *Data release 1 of the Dark Energy Spectroscopic Instrument*, arXiv:2503.14745 [INSPIRE].

[78] DESI collaboration, *DESI 2024 III: baryon acoustic oscillations from galaxies and quasars*, *JCAP* **04** (2025) 012 [arXiv:2404.03000] [INSPIRE].

[79] DESI collaboration, *DESI 2024 IV: baryon acoustic oscillations from the Lyman alpha forest*, *JCAP* **01** (2025) 124 [arXiv:2404.03001] [INSPIRE].

[80] DESI collaboration, *DESI DR2 results. I. Baryon acoustic oscillations from the Lyman alpha forest*, *Phys. Rev. D* **112** (2025) 083514 [arXiv:2503.14739] [INSPIRE].

[81] DESI collaboration, *DESI 2024 V: full-shape galaxy clustering from galaxies and quasars*, *JCAP* **09** (2025) 008 [arXiv:2411.12021] [INSPIRE].

[82] N. Schöneberg, *The 2024 BBN baryon abundance update*, *JCAP* **06** (2024) 006 [arXiv:2401.15054] [INSPIRE].

[83] DES collaboration, *The Dark Energy Survey: cosmology results with ∼1500 new high-redshift type Ia supernovae using the full 5 yr data set*, *Astrophys. J. Lett.* **973** (2024) L14 [arXiv:2401.02929] [INSPIRE].

[84] N.G. Karaçaylı et al., *DESI DR1 Lyα 1D power spectrum: the optimal estimator measurement*, *JCAP* **10** (2025) 004 [arXiv:2505.07974] [INSPIRE].

[85] C. Ravoux et al., *DESI DR1 Lyα 1D power spectrum: the Fast Fourier Transform estimator measurement*, *JCAP* **11** (2025) 079 [arXiv:2505.09493] [INSPIRE].

[86] eBOSS collaboration, *The Sloan Digital Sky Survey quasar catalog: fourteenth data release*, *Astron. Astrophys.* **613** (2018) A51 [arXiv:1712.05029] [INSPIRE].

[87] N. Palanque-Delabrouille et al., *Hints, neutrino bounds and WDM constraints from SDSS DR14 Lyman-α and Planck full-survey data*, *JCAP* **04** (2020) 038 [arXiv:1911.09073] [INSPIRE].

[88] M. Walther et al., *Emulating the Lyman-α forest 1D power spectrum from cosmological simulations: new models and constraints from the eBOSS measurement*, *JCAP* **05** (2025) 099 [arXiv:2412.05372] [INSPIRE].

[89] G. Rossi et al., *Suite of hydrodynamical simulations for the Lyman-α forest with massive neutrinos*, *Astron. Astrophys.* **567** (2014) A79 [arXiv:1401.6464] [INSPIRE].

[90] A. Borde et al., *New approach for precise computation of Lyman-α forest power spectrum with hydrodynamical simulations*, *JCAP* **07** (2014) 005 [arXiv:1401.6472] [INSPIRE].

[91] J. Torrado and A. Lewis, *Cobaya: code for Bayesian analysis of hierarchical physical models*, *JCAP* **05** (2021) 057 [arXiv:2005.05290] [INSPIRE].

[92] J. Torrado and A. Lewis, *Cobaya: Bayesian analysis in cosmology*, Astrophysics Source Code Library record ascl:1910.019, October 2019.

[93] A. Lewis, A. Challinor and A. Lasenby, *Efficient computation of CMB anisotropies in closed FRW models*, *Astrophys. J.* **538** (2000) 473 [astro-ph/9911177] [INSPIRE].

[94] C. Howlett, A. Lewis, A. Hall and A. Challinor, *CMB power spectrum parameter degeneracies in the era of precision cosmology*, *JCAP* **04** (2012) 027 [arXiv:1201.3654] [INSPIRE].

[95] F. James and M. Roos, *Minuit: a system for function minimization and analysis of the parameter errors and correlations*, *Comput. Phys. Commun.* **10** (1975) 343 [INSPIRE].

[96] H. Dembinski et al., *Scikit-hep/iminuit*, Zenodo, August 2023.

JCAP01(2026)041

[97] M. Chevallier and D. Polarski, *Accelerating universes with scaling dark matter*, *Int. J. Mod. Phys. D* **10** (2001) 213 [gr-qc/0009008] [INSPIRE].

[98] E.V. Linder, *Exploring the expansion history of the universe*, *Phys. Rev. Lett.* **90** (2003) 091301 [astro-ph/0208512] [INSPIRE].

[99] ATACAMA COSMOLOGY TELESCOPE collaboration, *The Atacama Cosmology Telescope: DR6 constraints on extended cosmological models*, *JCAP* **11** (2025) 063 [arXiv:2503.14454] [INSPIRE].

[100] DESI collaboration, *Cosmological implications of DESI DR2 BAO measurements in light of the latest ACT DR6 CMB data*, *Phys. Rev. D* **112** (2025) 083529 [arXiv:2504.18464] [INSPIRE].

[101] DESI collaboration, *The DESI experiment part I: science, targeting, and survey design*, arXiv:1611.00036 [INSPIRE].

[102] PLANCK collaboration, *Planck 2013 results. XVI. Cosmological parameters*, *Astron. Astrophys.* **571** (2014) A16 [arXiv:1303.5076] [INSPIRE].

[103] DES collaboration, *Dark Energy Survey: implications for cosmological expansion models from the final DES baryon acoustic oscillation and supernova data*, arXiv:2503.06712 [INSPIRE].

[104] D. Rubin et al., *Union through UNITY: cosmology with 2,000 SNe using a unified Bayesian framework*, *Astrophys. J.* **986** (2025) 231 [arXiv:2311.12098] [INSPIRE].

[105] DESI collaboration, *Extended dark energy analysis using DESI DR2 BAO measurements*, *Phys. Rev. D* **112** (2025) 083511 [arXiv:2503.14743] [INSPIRE].

[106] G. Efstathiou and S. Gratton, *The evidence for a spatially flat universe*, *Mon. Not. Roy. Astron. Soc.* **496** (2020) L91 [arXiv:2002.06892] [INSPIRE].

[107] S.-F. Chen and M. Zaldarriaga, *It's all ok: curvature in light of BAO from DESI DR2*, *JCAP* **08** (2025) 014 [arXiv:2505.00659] [INSPIRE].

[108] F. Couchot et al., *Cosmological constraints on the neutrino mass including systematic uncertainties*, *Astron. Astrophys.* **606** (2017) A104 [arXiv:1703.10829] [INSPIRE].

[109] L. Herold and M. Kamionkowski, *Revisiting the impact of neutrino mass hierarchies on neutrino mass constraints in light of recent DESI data*, *Phys. Rev. D* **111** (2025) 083518 [arXiv:2412.03546] [INSPIRE].

JCAP01(2026)041

Author List

D. Chebat[1], C. Yèche[1], E. Armengaud[1], N. Schöneberg[2,3], M. Walther[2,3], A. de Mattia[1], J. Rohlf[4], J. Aguilar[5], S. Ahlen[4], D. Bianchi[6,7], D. Brooks[8], T. Claybaugh[5], A. Cuceu[5], A. de la Macorra[9], P. Doel[8], S. Ferraro[5,10], A. Font-Ribera[11], J. E. Forero-Romero[12,13], E. Gaztañaga[14,15,16], G. Gutierrez[17], C. Hahn[18], H. K. Herrera-Alcantar[19,1], C. Howlett[20], D. Huterer[21,22], M. Ishak[23], J. Jimenez[11], R. Joyce[24], S. Juneau[24], R. Kehoe[25], D. Kirkby[26], A. Kremin[5], O. Lahav[8], A. Lambert[5], M. Landriau[5], L. Le Guillou[27], C. Magneville[1], M. Manera[28,11], R. Miquel[29,11], J. Moustakas[30], G. Niz[31,32], N. Palanque-Delabrouille[1,5], W. J. Percival[33,34,35], F. Prada[36], I. Pérez-Ràfols[37], G. Rossi[38], E. Sanchez[39], D. Schlegel[5], J. Silber[5], D. Sprayberry[24], G. Tarlé[22], B. A. Weaver[24], P. Zarrouk[27], R. Zhou[5], H. Zou[40]

[1] *IRFU, CEA, Université Paris-Saclay, F-91191 Gif-sur-Yvette, France*
[2] *University Observatory, Faculty of Physics, Ludwig-Maximilians-Universität, Scheinerstr. 1, 81677 München, Germany*
[3] *Excellence Cluster ORIGINS, Boltzmannstrasse 2, D-85748 Garching, Germany*
[4] *Department of Physics, Boston University, 590 Commonwealth Avenue, Boston, MA 02215 U.S.A.*
[5] *Lawrence Berkeley National Laboratory, 1 Cyclotron Road, Berkeley, CA 94720, U.S.A.*
[6] *Dipartimento di Fisica "Aldo Pontremoli", Università degli Studi di Milano, Via Celoria 16, I-20133 Milano, Italy*
[7] *INAF-Osservatorio Astronomico di Brera, Via Brera 28, 20122 Milano, Italy*
[8] *Department of Physics & Astronomy, University College London, Gower Street, London, WC1E 6BT, U.K.*
[9] *Instituto de Física, Universidad Nacional Autónoma de México, Circuito de la Investigación Científica, Ciudad Universitaria, Cd. de México C. P. 04510, México*
[10] *University of California, Berkeley, 110 Sproul Hall #5800 Berkeley, CA 94720, U.S.A.*
[11] *Institut de Física d'Altes Energies (IFAE), The Barcelona Institute of Science and Technology, Edifici Cn, Campus UAB, 08193, Bellaterra (Barcelona), Spain*
[12] *Departamento de Física, Universidad de los Andes, Cra. 1 No. 18A-10, Edificio Ip, CP 111711, Bogotá, Colombia*
[13] *Observatorio Astronómico, Universidad de los Andes, Cra. 1 No. 18A-10, Edificio H, CP 111711 Bogotá, Colombia*
[14] *Institut d'Estudis Espacials de Catalunya (IEEC), c/ Esteve Terradas 1, Edifici RDIT, Campus PMT-UPC, 08860 Castelldefels, Spain*
[15] *Institute of Cosmology and Gravitation, University of Portsmouth, Dennis Sciama Building, Portsmouth, PO1 3FX, U.K.*
[16] *Institute of Space Sciences, ICE-CSIC, Campus UAB, Carrer de Can Magrans s/n, 08913 Bellaterra, Barcelona, Spain*
[17] *Fermi National Accelerator Laboratory, PO Box 500, Batavia, IL 60510, U.S.A.*
[18] *Steward Observatory, University of Arizona, 933 N. Cherry Avenue, Tucson, AZ 85721, U.S.A.*
[19] *Institut d'Astrophysique de Paris. 98 bis boulevard Arago. 75014 Paris, France*
[20] *School of Mathematics and Physics, University of Queensland, Brisbane, QLD 4072, Australia*
[21] *Department of Physics, University of Michigan, 450 Church Street, Ann Arbor, MI 48109, U.S.A.*
[22] *University of Michigan, 500 S. State Street, Ann Arbor, MI 48109, U.S.A.*
[23] *Department of Physics, The University of Texas at Dallas, 800 W. Campbell Rd., Richardson, TX 75080, U.S.A.*
[24] *NSF NOIRLab, 950 N. Cherry Ave., Tucson, AZ 85719, U.S.A.*
[25] *Department of Physics, Southern Methodist University, 3215 Daniel Avenue, Dallas, TX 75275, U.S.A.*
[26] *Department of Physics and Astronomy, University of California, Irvine, 92697, U.S.A.*

JCAP01(2026)041

[27] *Sorbonne Université, CNRS/IN2P3, Laboratoire de Physique Nucléaire et de Hautes Energies (LPNHE), FR-75005 Paris, France*
[28] *Departament de Física, Serra Húnter, Universitat Autònoma de Barcelona, 08193 Bellaterra (Barcelona), Spain*
[29] *Institució Catalana de Recerca i Estudis Avançats, Passeig de Lluís Companys, 23, 08010 Barcelona, Spain*
[30] *Department of Physics and Astronomy, Siena College, 515 Loudon Road, Loudonville, NY 12211, U.S.A.*
[31] *Departamento de Física, DCI-Campus León, Universidad de Guanajuato, Loma del Bosque 103, León, Guanajuato C. P. 37150, México*
[32] *Instituto Avanzado de Cosmología A. C., San Marcos 11 — Atenas 202. Magdalena Contreras. Ciudad de México C. P. 10720, México*
[33] *Department of Physics and Astronomy, University of Waterloo, 200 University Ave W, Waterloo, ON N2L 3G1, Canada*
[34] *Perimeter Institute for Theoretical Physics, 31 Caroline St. North, Waterloo, ON N2L 2Y5, Canada*
[35] *Waterloo Centre for Astrophysics, University of Waterloo, 200 University Ave W, Waterloo, ON N2L 3G1, Canada*
[36] *Instituto de Astrofísica de Andalucía (CSIC), Glorieta de la Astronomía, s/n, E-18008 Granada, Spain*
[37] *Departament de Física, EEBE, Universitat Politècnica de Catalunya, c/Eduard Maristany 10, 08930 Barcelona, Spain*
[38] *Department of Physics and Astronomy, Sejong University, 209 Neungdong-ro, Gwangjin-gu, Seoul 05006, Republic of Korea*
[39] *CIEMAT, Avenida Complutense 40, E-28040 Madrid, Spain*
[40] *National Astronomical Observatories, Chinese Academy of Sciences, A20 Datun Road, Chaoyang District, Beijing, 100101, P. R. China*

JCAP01(2026)041